DEUTSCHES ELEKTRONEN – SYNCHROTRON DESY

DESY 90-136
LAPP-EXP-90.11
LAL 90.68
IC/HEP/90/11
November 1990

Calorimetry at the LHC

J. Colas

Lab. de Physique des Particules (LAPP), Annecy

R. Klanner

Deutsches Elektronen-Synchrotron DESY, Hamburg

J.P. Repellin

Lab. de l'Accélérateur Linéaire (LAL), Orsay

T.S. Virdee

Imperial College London

ISSN 0418-9833

NOTKESTRASSE 85 · 2 HAMBURG 52

To be sure that your preprints are promptly included in the
HIGH ENERGY PHYSICS INDEX ,
send them to the following address (if possible by air mail) :

DESY
Bibliothek
Notkestrasse 85
2 Hamburg 52
Germany

DESY 90-136
LAPP-EXP-90.11
LAL 90.68
IC/HEP/90/11
November 1990

ISSN 0418-9833

CALORIMETRY AT THE LHC

J. Colas[1], R. Klanner[2], J.P. Repellin[3], T.S. Virdee[4]

LAPP Annecy[1] - DESY Hamburg[2] - LAL Orsay[3] - Imperial College London[4]

Large Hadron Collider Workshop, Aachen , October 1990

Calorimetry plays an important role in the present high energy hadron collider experiments in identifying and measuring the energies of electrons, reconstructing and measuring the energies of jets and detecting non-interacting particles via missing transverse energy. This will become even more so at the LHC and the SSC. Only calorimeters have resolutions that improve with increasing energy with only a moderate increase in the detector depth. They can also cope with the high particle densities expected at the future colliders. As at the present colliders, leptons at high transverse momenta are expected to sign new particles and new physics. Electromagnetic calorimeters with a large dynamic range will play an especially important role.

The new challenges that the calorimeters at the LHC will have to face are :

- luminosities in excess of 10^{34} $cm^{-2}s^{-1}$ with inter-bunch crossing times of ~15 ns, requiring radiation hardness and speed of response far beyond what has so far been achieved,
- performance at high energies will be dominated more by instrumental deficiencies such as non-uniformity of response, finite containment, inter-cell calibration etc. than by intrinsic calorimeter resolution thus requiring much better control of the systematic effects,
- the calorimeters will have to provide, at different levels of triggers, rejection factors that are several orders of magnitude in the presence of very large interaction rate ($\geq 10^9$ s^{-1}),
- large calorimeter volumes and the large number of readout channels will require new designs for the mechanics and the electronics.

It is the first point that at present appears to be the most difficult, important and urgent to address. Thus a significant part of this report is devoted to it.

Calorimetry at the future hadron colliders has been the subject of several workshops [1]. Last year ECFA organized a study week on Instrumentation Technology for High Luminosity Hadron Colliders in Barcelona [2]. Since then the study of the required detector performance and the experimental R&D has intensified.

The Calorimeter Working Group of this workshop was formed in April 1990. In order to define the performance criteria necessary for the extraction of the physics signals, usually in the presence of large backgrounds, the subgroup "Physics versus Calorimeter Performance" convened by J. P. Repellin, worked closely with the Physics Working Group. This work is summarized in section 1.

The Calorimeter Working Group devoted much time to the evaluation of the different calorimeter techniques with a view of their use at luminosities of 10^{34} $cm^{-2}s^{-1}$ and higher. We present here a summary of the contributions made by a large number of people during the last six months. The questions asked of each technique were :

- What is the radiation sensitivity ?
- What is the signal shape and the effect of pileup ?
- What are the measurement resolutions (energy, position) for electrons, hadrons and hadron jets, what is the linearity of response ?
- What calibration accuracy can be achieved ?
- What is the achievable segmentation ?
- What hermeticity can be attained ?
- What level of particle (electron) identification can be achieved ?
- Is the technique affected by a magnetic field ?
- What is the level of the maturity of the technique ?
- What is the estimated R&D effort required and the time required in order to be able to reach a decision on suitability at the LHC ?

At the first working group meeting in April, subgroups for the following techniques were formed (persons in parentheses took over the work in the cases where the convenor could not attend the Aachen meeting) :

Sampling Calorimeters (em/had) :	Subgroup Convenors:
Scintillator Tiles-Wavelength Shifter	H.Tiecke, (R.Klanner)
Scintillating Fibers	L. Poggioli
Liquid Argon	D. Fournier
Room Temperature Liquids	E. Radermacher
Silicon	G. Lindstroem
Homogeneous EM Calorimeters :	
Crystals	H. Newman, (P.Lecoq)
Noble Liquids	T. Virdee

The subgroups met independently and reported regularly at the working group meetings and finally during the first three days of the Aachen Workshop. Section 2 summarizes this work and short conclusions are given at the end of each of the sub-sections dealing with the individual calorimeter techniques. More details can be found in the sub-convenor reports in

Vol.3 of these proceedings. Section 2 also briefly summarizes the performance parameters relevant for the front-end electronics chain and recalls the radiation levels that the calorimeters will have to stand.

1. PHYSICS REQUIREMENTS

1.1 Cross-sections

Most of the physics reactions of interest at the LHC have low cross-sections. For example, the production cross-section for a Higgs boson, a new Z or a new W are in the picobarn range whereas the total cross section is of the order of 100 mb. Furthermore the inclusive jet cross-section for a jet with a transverse momentum larger than 20 GeV/c is about 300 μb. This QCD background is many orders of magnitude larger than most of the signals of interest. This leads to an emphasis on the leptonic signatures. They provide a large rejection factor against the QCD backgrounds but at the price of a loss in rate due to the smallness of the leptonic or semileptonic branching ratios eg. BR(W -> ev) or B(t -> evb) are both ~10% and BR(Z -> ee) ~ 3%. As an example, Fig. 1 shows the σ.BR(H -> ZZ -> 4 l) where l = e or μ. It is about 10 fb for a Higgs with a mass of 400 GeV [3,4]. The σ.BR(H -> γγ) is shown in Fig. 2 and has a similar value [3,5].

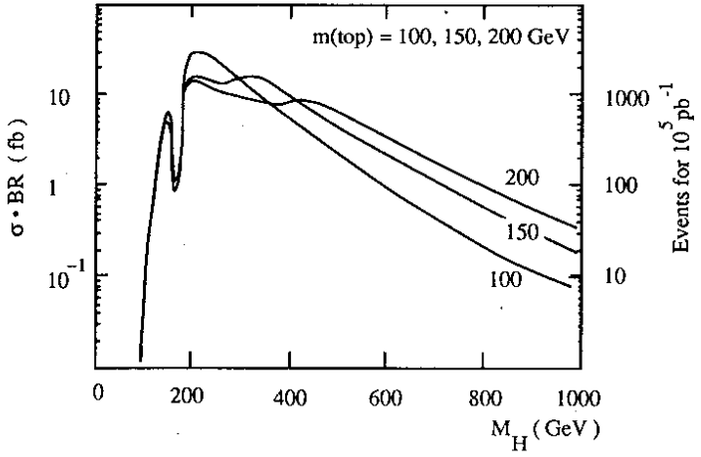

Figure 1 : Cross-section times branching ratio for the 4 lepton decay of the Higgs : H-> ZZ -> 4 l where l = e or μ. The number of events shown are for an integrated luminosity of 10^5 pb^{-1}

The observation of signals with such low cross-sections requires a high luminosity, perhaps in excess of 10^{34} $cm^{-2}s^{-1}$. Consequently we have set the benchmark at a luminosity of 2.10^{34} $cm^{-2}s^{-1}$ and 15 ns between crossings. This necessarily introduces a bias to the conclusions as they may be different for a lower luminosity running and should thus be borne in mind throughout the rest of the report.

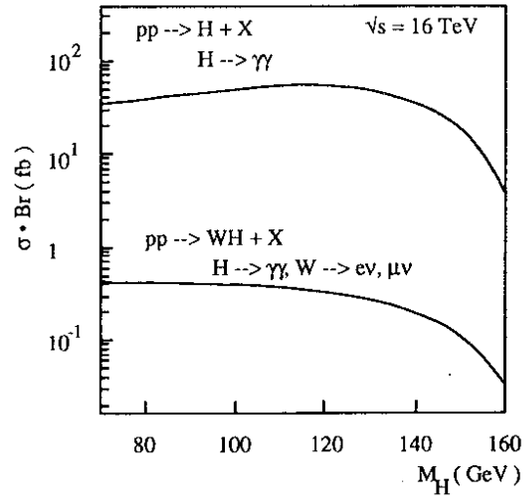

Figure 2 : Cross-section times branching ratio for the H -> 2 γ decay as function of the Higgs mass.

1.2 Acceptance : Rapidity Coverage and Transverse Momentum Thresholds.

Heavy objects in high energy pp collisions are preferentially produced at central rapidities. This usually applies also to their decay products. In this section, a few processes are used to investigate the extent of rapidity coverage that is required.

1.2.1 H -> ZZ -> eeee

This process, with a striking signature, requires a large rapidity coverage and the measurement of electrons with low transverse momenta [4]. A large acceptance is needed as both the production cross-section and the Z branching ratio into electron pairs is small. The acceptance as a function of the transverse momentum of the electron having the smallest p_t is shown in Fig.3 for three different Higgs masses and for a rapidity coverage of ± 3 units. These curves indicate that the observation of a low mass Higgs requires the detection of electrons with transverse momenta as low as 10 GeV/c. This is also true of the search for SUSY particles which have cascade decay chains leading to electrons. The same figure shows the acceptance of the leptons from the decays of Z's produced in the process $\tilde{g}\tilde{g}$ -> $\tilde{\chi}\tilde{\chi}$ + X -> ZZ + X -> 4 l + X with a gluino of a mass of 1 TeV/c^2 and for the full rapidity coverage [6].

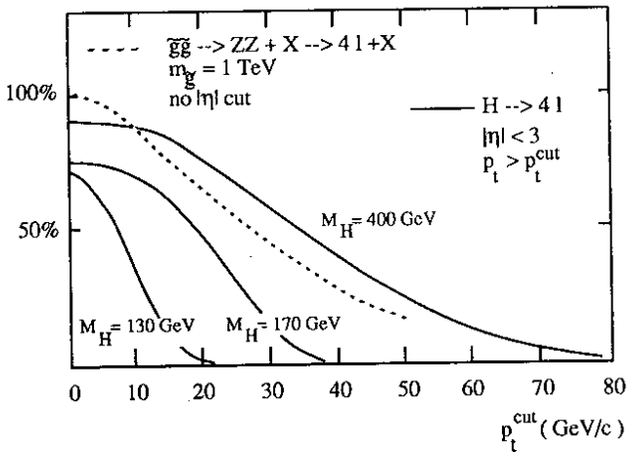

Figure 3 : Acceptance as function of the transverse momentum of the electron having the smallest p_t for two physics processes : H -> 4 e and $\tilde{g}$ -> Z + X -> 2e + X.

Table 1 summarizes the acceptance, for the process H -> ZZ -> 4 l, of a calorimeter for 3 values of the Higgs mass (140, 200 and 500 GeV/c^2). The first column gives the acceptance of an electron pair trigger with a p_t cut of 20 GeV/c. This shows that such a trigger maintains a reasonable acceptance for a low mass Higgs boson even if the acceptance is limited to ± 2 units of rapidity. As can be seen from the last two columns, a low p_t threshold for the lepton with the smallest p_t is crucial for detecting a low mass Higgs. The geometrics acceptance grows almost linearly with the rapidity coverage. An electromagnetic calorimeter with a rapidity coverage between ± 2 and ± 3 units is clearly desirable.

	|η|	$P_t^{l2} > 20$ GeV	$P_t^{l4} > 10$ GeV	$P_t^{l4} > 20$ GeV
M_H = 140 GeV	<3	.91	.54	.11
	<2	.67	.33	.07
M_H = 200 GeV	<3	.94	.76	.56
	<2	.73	.48	.38
M_H = 500 GeV	<3	.98	.88	.80
	<2	.82	.62	.57

Table 1 : Acceptance for the H -> $ZZ^{(*)}$ -> 4 *l* decay channel as function of the angular coverage and transverse momentum cut on the electrons (see text).

1.2.2 H -> γγ

Studies of this mode [5] show that a calorimeter coverage of ± 2 units of rapidity provides an adequate acceptance for Higgs masses around 100 GeV/c^2. Fig. 4 shows the p_t distribution of the photon with the higher and the lower p_t. An asymmetric cut on the p_t of the two photons is used to reject the background. Cuts set at 40 GeV/c and 25 GeV/c for the two photons within a rapidity range of ± 2 units lead to an acceptance of 41% for M_H = 100 GeV/c^2 and 51% for M_H = 150 GeV/c^2. Extending the coverage to ± 3 units increases the signal acceptance, after p_t cuts, by 45%. The background, however is increased by more than 50% resulting in a gain in the significance of 18%.

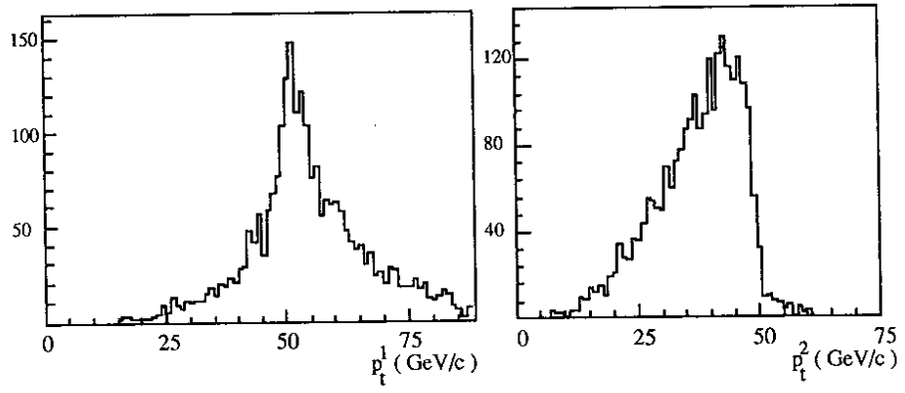

Figure 4 : H -> γγ : Transverse momentum distribution of the photon with the higher and lower p_t for a Higgs with a mass of 100 GeV/c^2.

1.2.3 Tagging of IVB fusion process

For Higgs masses larger than ~ 700 GeV and depending on the mass of the top quark the IVB fusion production mechanism competes with the gluon fusion process. Consequently identification of the two very forward quark jets can be used to identify events from the IVB fusion process and thus extend the detectability of the Higgs boson to higher masses.

The rapidity distribution of the "tagging" jets and the energy distribution of the jet with the lower energy are shown in Fig 5 [7]. In order to be sensitive to this process the coverage of a hadronic calorimeter has to extend to rapidities up to at least ± 4 units. This calorimeter will have to survive a very high level of radiation. However the calorimeter performance does not have to be very good as the jets have very high energies and are well collimated.

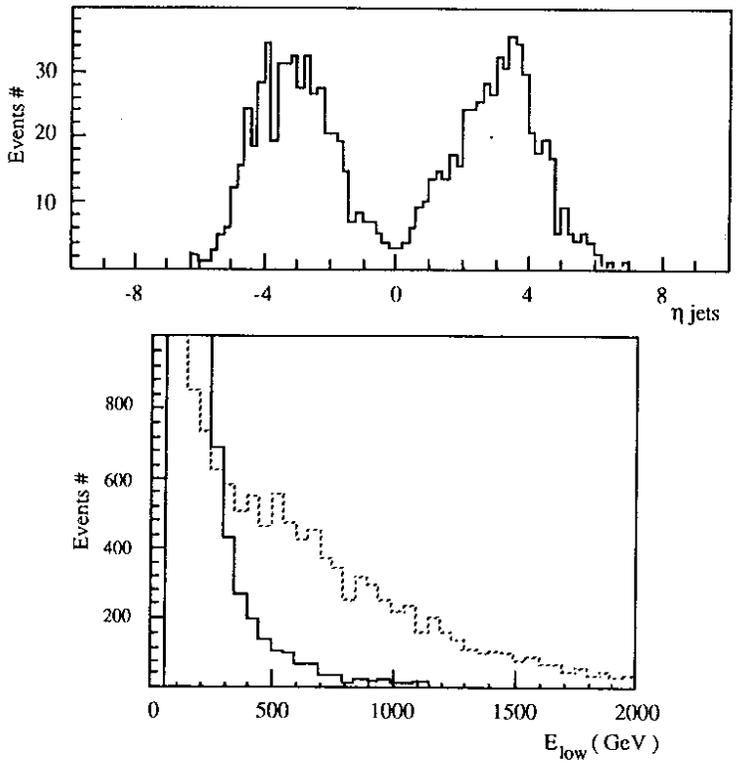

Figure 5 : Rapidity distribution of the "tagging" jets and energy distribution of the lower energy jet for the WW fusion process pp -> qqH. Dashed line is the signal and the full line is the QCD background.

1.3 Missing Transverse Energy.

The observation of an imbalance in the transverse momentum is an important signature for the presence of non-interacting particles eg. a neutrino or the lightest supersymmetric particle. The usefulness of such a signature, based on a cut on the missing transverse momentum, depends on the process under study, the particular backgrounds that fake the signal and the coverage and the performance of the calorimeter. We examine these points by considering a few examples.

1.3.1 H -> ZZ (Z -> ee, Z -> νν)

This reaction is of interest for large Higgs masses (≥ 500 GeV/c^2) where the larger branching fraction of the Z -> 2ν can be used to extend the range of sensitivity. The identification relies on the observation of one Z decaying into electrons (with for example p_t^Z > 100 GeV/c) accompanied by a large missing p_t. The signal appears as a Jacobian peak in the p_t^Z distribution above an irreducible background from Z pair production. However this assumes that the huge background from Z + jets events, where the jets are mismeasured or are outside the calorimeter

acceptance, can be rejected. The level of this background is shown in Fig. 6 as a function of the missing p_t for different rapidity coverages (± 2, ± 3, ± 4 units) [4]. A rapidity coverage of ± 4 units is essential for the observation of this process.

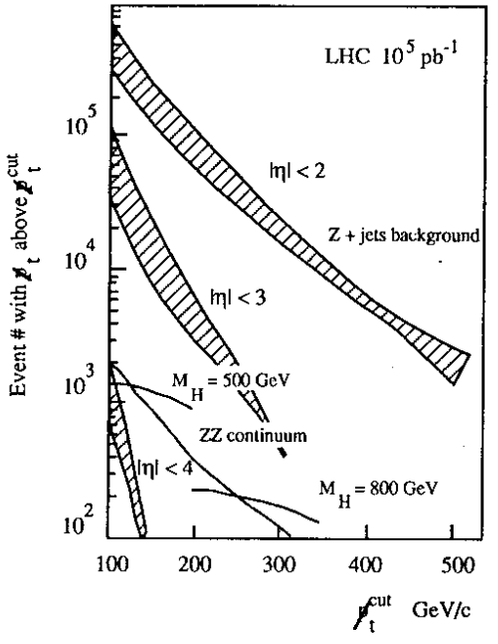

Figure 6 : Missing transverse momentum distribution for the H -> ZZ -> eevν signal and for backgrounds from the ZZ continuum and from Z+jets events, as a function of the calorimeter coverage.

1.3.2 pp -> t t̄ -> eν + jets

The observation of t t̄ pair production with a top quark decaying semi-leptonically requires a rejection factor of ~ 10^5 against jets faking electrons. The effectiveness of a cut on the missing transverse momentum has been studied to see whether the level of rejection required can be relaxed [8]. Fig. 7 shows, for M_{top} = 130 GeV/c^2, the rejection obtained by the cuts p_t^{miss} ≥ 50 GeV/c (upper set of curves) and p_t^{miss} ≥ 100 GeV/c (lower set of curves). For p_t^{miss} ≥ 50 GeV/c the rejection factor that can be obtained is ~ 10 - 100 depending on the rapidity coverage. A large rapidity coverage |η| ≥ 4 units seems necessary though the rejection power comes at the price of a loss of acceptance (crosses) and is considerably affected by the pile-up from 20 minimum bias events. But a higher p_t^{miss} cut leads to a substantial loss in acceptance.

The pile-up from minimum bias events at high luminosity widens the missing p_t distribution. To reduce the apparent missing p_t from the fluctuation in the minimum bias pileup only jets exceeding some p_t threshold could be used in the computation of p_t^{miss}. The effect is then limited to the smearing of the energy in the cells used for the jet energy reconstruction and to the

fluctuation in the number of jets which pass the p_t threshold. Quantitative estimates thus require specific simulation for each process.

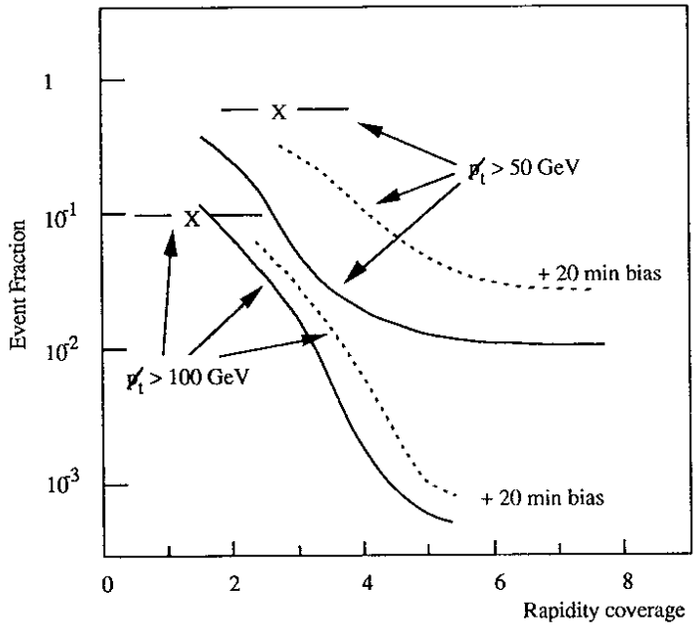

Figure 7 : Acceptance for the process $t\bar{t}$ -> ev + jets and the QCD background rejection factor for two cuts on the missing transverse momentum, as a function of the calorimeter coverage.

1.3.3 p_t^{miss} for events with ≥ 3 jets.

A study of the p_t^{miss} distribution of 3 jet events has been made in the context of the search for supersymmetric particles [9,10]. A procedure has been developed to simulate the energy smearing and the lateral development of jets. Fig. 8 shows that a deterioration of the energy resolution of the calorimeter from 40% /√E to 80% /√E would correspond to a shift of a p_t^{miss} cut from 120 GeV/c to 160 GeV/c [9]. The pile-up from minimum bias events was not included in this simulation.

The interplay between the effects of limited calorimeter coverage, energy resolution, energy losses in cracks and event pileup has still to be studied in depth.

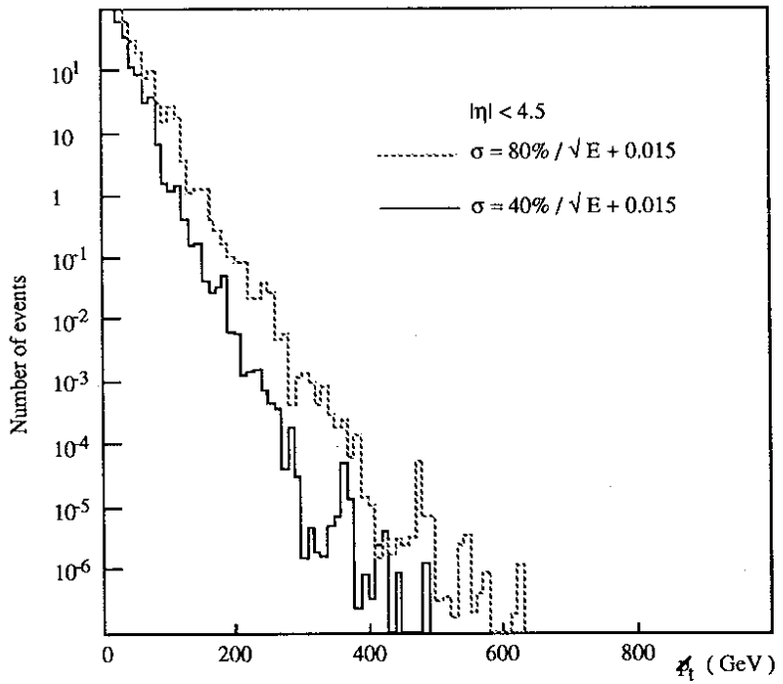

Figure 8 : Distribution of missing transverse momentum for 3-jet events as a function of the calorimeter resolution. Pileup is not included.

1.4 Pileup, Detector Speed and Calorimeter Granularity

At a luminosity of 2.10^{34} $cm^{-2}s^{-1}$ there are ~ 20 inelastic pp interactions in each bunch crossing. Hence even an ideally fast calorimeter will suffer pileup. Moreover, hadronic shower development is not instantaneous but requires at least ≈ 45 ns, as measured by the SPACAL collaboration in the scintillating fiber calorimeter [11]. Low energy neutrons in the hadronic shower are moderated by collisions with essentially free protons in the plastic fibers with a time constant of the order of ≈ 10 ns (Fig. 9).

The vast majority of hadronic collisions which constitute the pileup produce particles with low transverse momenta with the spectrum being parametrized by :

$$\frac{dN}{dp_t} = p_t e^{-bp_t} \text{ with } \langle p_t \rangle \approx 0.65 \text{ GeV/c} \qquad (1)$$

with an average number of 10 charged and neutral particles per unit of rapidity.

The particles from the overlapping events will contribute to the energy measured in the calorimeter. The calorimeter energy resolution is thus degraded although their average contribution can be subtracted.

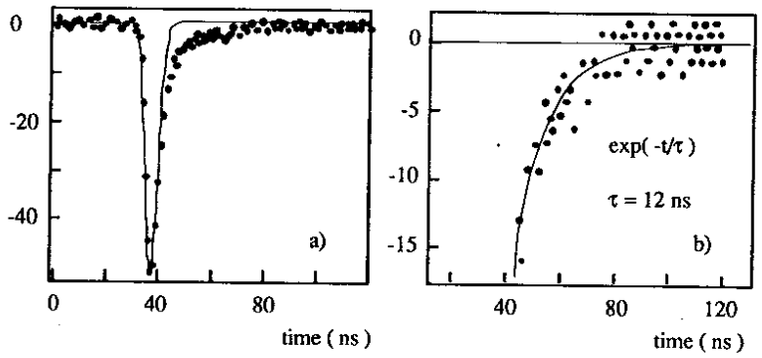

Figure 9 : A typical pulse from a 150 GeV pion shower in the SPACAL fiber calorimeter. The pulse is nearly Gaussian a) with an exponential tail toward large time presumed to be due to low energy neutrons. The late part of the pulse is expanded in b).

1.4.1 Pile-up and Jets

Present collider experiments usually measure the energy of a jet by summing the energy contained in cells in a rather large cone, of half-angle $\Delta R = \sqrt{(\Delta\eta^2 + \Delta\phi^2)} \sim 0.7$ -1.0. For the LHC, the studies at high luminosities (2.10^{34} cm^{-2}s^{-1}) show that ΔR has to be reduced to ≤ 0.4. Small cone sizes cut hard into the jet core but larger ones sum over too much pile-up. Fig.10 shows the distribution of the transverse energy piling into a cone of half-angle $\Delta R=0.4$ as estimated from equation (1). This is computed for two types of detectors, an ideally fast calorimeter which is sensitive to only one crossing and a "slow" one which integrates over 60ns i.e. four crossings. The two distributions are nearly Gaussian as expected from the fact that ≈ 20 particles per crossing deposit their energy into the cone. The pileup can be considered as an additional source of noise once the average value of this contribution is subtracted. Assuming no short range correlations eg. from jets, the dependence of the average and the r.m.s. values of these distributions with luminosity, cell size and detector sensitive time (τ) are given by:

$$\langle \text{pileup} \rangle \propto \langle p_t \rangle \cdot \text{Luminosity} \cdot \text{area} \cdot \tau \qquad (2)$$

$$\langle \sigma_{\text{pileup}} \rangle \propto \langle p_t \rangle \cdot \sqrt{\text{Luminosity} \cdot \text{area} \cdot \tau}$$

For a hadronic calorimeter with 45ns integration time using a cone of a half-angle of $\Delta R=0.4$, the r.m.s. of the pile-up energy ($\sigma_E \geq 6.2$ GeV) sets a lower limit on the jet energy resolution that corresponds to ~60% / $\sqrt{E_T}$ for a 100 GeV jet. This however is a small effect for very high energy jets ($E \geq 1$ TeV) as the constant term will probably dominate the hadronic energy resolution.

More work is needed to fully understand the effect of pile-up on missing transverse momentum although some work has already been done for the detection of the top quark [8] and for the search for SUSY particles [6]. It should also be noted that calorimeter triggers will preferentially pick up events with large pile-up and thus worsen the situation. This also has to be studied more carefully.

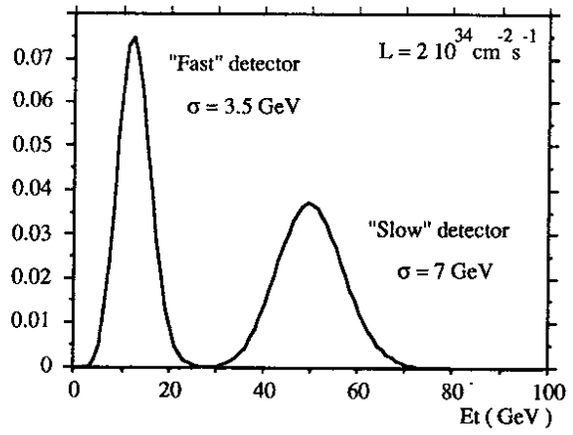

Figure 10 : Distribution of the transverse energy from minimum bias events piling up in a cone of half opening angle $\Delta R=0.4$ for a luminosity of 2.10^{34} cm^{-2}s^{-1} . Two types of detector are considered : a "fast" one which can resolve two crossings and a "slow" one which integrates over 4 crossings.

1.4.2 Pile-up and Photons, Electrons

Electromagnetic showers have a much smaller transverse size: ≈ 90% of their energy is contained in a cylinder with a diameter of ~ 5 X_0 (i.e. 4 - 15 cm depending on the calorimeter characteristics). The average number of particles from minimum bias events in such a small region is smaller than unity and pileup is not Gaussian anymore. Consider a typical calorimeter having a σ_E = 400 MeV for 20 GeV electrons (i.e. ~9% /$\sqrt{E}$). Assume a lateral segmentation into square cells which are large enough to contain the electromagnetic shower. Then the probability to have less than 400 MeV from event pile-up can be computed using equation (1). Fig. 11 shows that, at $L = 2.10^{34}$ cm^{-2}s^{-1} , 30% of the events will have more than the 400 MeV of pileup energy in a cell of $\Delta\eta\Delta\phi \approx .12^2$ in the case of a fast calorimeter. A size of $\Delta\eta\Delta\phi \approx 0.06^2$ is required for a "slow" detector in order to get the same result. Good granularity is thus very important for an LHC calorimeter which aims to measure electron or photon energies precisely. Note that the true granularity has to be ≥ 3 times better in order to take into account particles falling near cell boundaries and for the calorimetric measurement of the electron/photon impact point.

The lateral size of the shower determines the containment radius for a given electromagnetic calorimeter. This can be used to put a lower limit on the inner radius needed for that calorimeter so that the energy resolution not be degraded by pileup. For example: if at a luminosity of 2.10^{34} cm^{-2}s^{-1} only 10% of the events are allowed to have pileup energy ≥ 400 MeV in an area of a size of ~ 10 x 10 cm^2, then the inner radius should be ≥ 1.4 m.

Pile-up sets a limit on the effectiveness of the electron/photon isolation criteria and also spoils the reconstruction of shower position (which is useful to identify electrons using the spatial matching with a charged track). Again this sets constraints on the calorimeter granularity and will be discussed below in section 1.6.1.

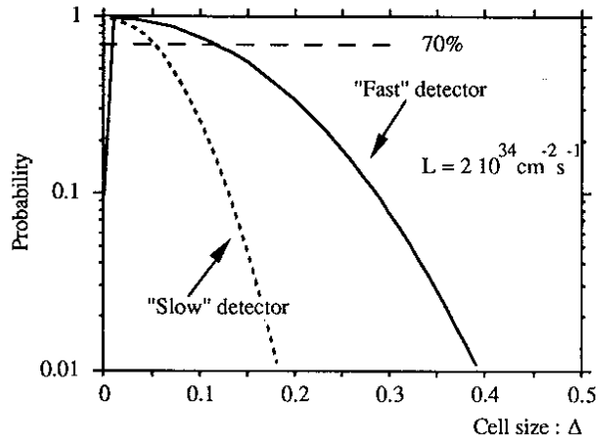

Figure 11 : Fraction of events with less than 400 MeV piled-up in a square cell of size $\Delta\eta\Delta\phi=\Delta^2$ for a 2.10^{34} $cm^{-2}s^{-1}$ luminosity. Two types of detector are considered : a "fast" one which can resolve each crossing and a "slow" one which integrates over 4 crossings.

1.5 Trigger on Electrons and Photons

The importance of the detection of charged leptons and photons in the search for new heavy particles was stressed in section 1.1. Calorimeters thus need to be able to trigger on events containing electrons and photons with high transverse momenta. This provides the first level of suppression of the large background resulting from QCD interactions. Some of the implications of such a requirement are considered below.

Consider a trigger based on an electron from the semi-leptonic decay of one of the top quarks in the reaction pp -> $t\bar{t}$ where t -> Wb -> evb [8]. The acceptance for such an electron with $p_t > 40$ GeV/c, in a rapidity range $|\eta| \leq 2$, is 33% (52%) if the mass of the top quark is 100 (200) GeV/c^2. Although both the acceptance and the production cross-sections (10nb for M_t=100 GeV/c^2 and 0.7nb for M_t=200 GeV/c^2) for the top quark are large, the inclusive jet cross-section for the same kinematic cuts is ~ 50μb which would give a trigger rate of 50 kHz at a luminosity of 10^{33} cm^{-2} s^{-1}. A reduction of this rate by 2 orders of magnitude is needed from the first two levels of trigger [12]. At a luminosity of 2.10^{34} cm^{-2} s^{-1} either the rejection factor has to be ~1000 or the p_t threshold has to be raised to 100 GeV/c for the same rate of inclusive electron triggers. This can be compared with a reduction of 5-6 orders of magnitude required offline to take the background below the level of the signal.

1.5.1 Single Electromagnetic Cluster Trigger.

From the discussion above it can be seen that the calorimeter has to provide, at the trigger level, a rejection of a factor of ~ 100 or more against jets.

A first rejection factor comes from the requirement of a threshold on the transverse energy deposited in the electromagnetic part of the calorimeter. A thickness of 25-30 radiation lengths is required to collect the energy of high energy electron or photon showers. The jets also deposit a sizeable fraction of their energy in such a thickness but it is considerably less localized as compared with single electron or photon energy deposits. This characteristic has already been used in the present generation of collider experiments. GEANT simulations show that a rejection factor of ~ 50-100 against jets [13] can be expected for a threshold of $p_t \geq$ 20 GeV/c for a "cell" with dimensions $\Delta\eta.\Delta\phi = 0.1^2$. This rejection has a weak dependence on the cell size and can be roughly parametrized as $1/\sqrt{(\Delta\eta.\Delta\phi)}$. This rejection is still smaller than the jet/π^0 ratio which is ~ 200 at p_t ~ 20 GeV/c (Fig. 13).

A further rejection can be obtained by requiring that the e.m. energy deposit be isolated. This is effected by allowing only a limited amount of energy in the electromagnetic cells surrounding and in the hadronic cells behind the trigger cells. The above mentioned GEANT simulations show that an overall rejection factor of ~ 1000 can be attained for an electron inefficiency of less than 5% in a fast calorimeter and about 10% in the "slow" calorimeter defined in 1.4.1.

1.5.2 Electromagnetic Pairs Trigger

As explained in section 1.2, the calorimeter has to provide the trigger for H -> 2γ or H -> ZZ (Z -> ee) channels. A p_t threshold no higher than ~ 20 GeV/c is required to have a sizeable acceptance for a low mass Higgs boson.

The cross-section for 2 jet production, with both jets having a $p_t \geq$ 20 GeV/c and within a rapidity range $|\eta| \leq 2$, is ~ 330 μb. Including the effect of pileup, which becomes significant at a luminosity of 10^{34} cm^{-2} s^{-1}, leads to a 2 jet rate of ~10 MHz. However the electromagnetic trigger is less affected by pileup, as compared to a jet trigger, and an online rejection of a factor of ~ 100 per leg brings the trigger rate down to ~300 Hz which can then be handled by the 2nd level trigger. It should be noted that the σ.BR(Z->ee) ~ 1 nb for a rapidity coverage of $|\eta| \leq 2$ leading to a di-electron rate of ~ 10 Hz at L = 10^{34} cm^{-2} s^{-1}. A large number of events can thus be accumulated in a relatively short time and may enable the precise calibration of an electromagnetic calorimeter. Various other processes eg. SUSY particle decays having Z's in their decay cascades, ZZ and ZW production also require such a di-e.m. shower trigger.

1.6 Calorimetric Identification of Electrons and Photons

Except for a limited number of processes involving more than 2 leptons, the rejection factor of ~ 1000 against jets is not sufficient to reduce the QCD background to the levels of irreducible

backgrounds. For example, in the channel pp -> t $\bar{t}$ -> eν + jets, a jet rejection of the order of 10^5-10^6 is required. In this section we consider what rejection factors can be attained by calorimeters.

1.6.1 Electron Identification

A charged track pointing to an electromagnetic shower is obviously the minimum that is required for the shower to be identified with an electron. This signature can however be faked by eg. a charged track overlapping with a π^0, a hadron showering like an electron.

The difference between the development of electromagnetic and hadronic showers, both laterally and longitudinally can be used to distinguish electrons from charged hadrons. The UA1 collaboration has shown that given a sufficient longitudinal and lateral segmentation a charged hadron rejection factor of ~ 10^4 for single high energy showers can be attained for an electron efficiency of 90 % [14]. The effect of pileup and the rejection in jets has not been studied during this workshop.

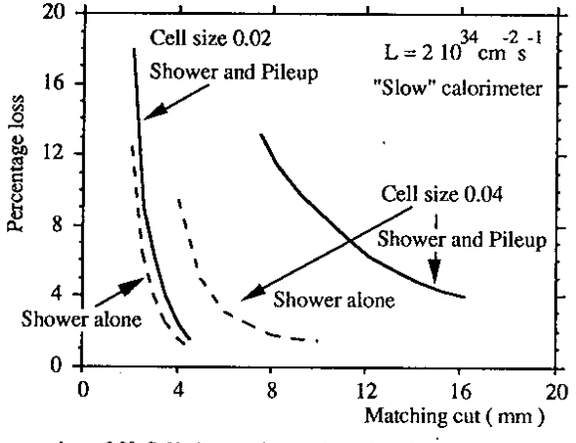

Figure 12 : Percentage loss of 20 GeV electron due to charged track - calorimeter impact mismatch as a function of mismatch distance. Pileup effect becomes substantial for coarse calorimeter granularity. This is computed for the "slow" calorimeter defined in 1.4.1, with an effective radiation length of 1.1 cm.

The lateral development of an electron shower can be used to determine the position of the impact which can then be compared with the position given by the extrapolation of a track found by a tracking device. The calorimeter-track matching has been used by experiments at present hadron colliders to reject charge track-π^0 overlaps. In a high luminosity environment the effectiveness of this method is compromised by pileup. GEANT simulation has been done to study this problem [13]. The results are summarized in Fig. 12 which shows the loss of showers with p_t = 20 GeV/c as a function of the maximum distance allowed between the extrapolated track and the shower position. It can be seen that the maximum distance is ~ 3mm

for a 5% loss in efficiency and is not too dependent on pileup as long as the calorimeter cell size is kept smaller than $\Delta\eta.\Delta\phi = 0.02^2$. For larger cell sizes eg $\Delta\eta.\Delta\phi = 0.04^2$ this distance has to be substantially increased (to 14 mm) in order to maintain the same efficiency and the pileup substantially degrades the matching precision. These simulations were done with a simple model for a calorimeter with an inner radius of 1m and a radiation length of 1.1 cm.

The rejection factor against jets obtained by track-shower match depends on the type of background. It is effective against accidental overlap of a high energy π^0 and a charged track from either a jet or a minimum bias event. This background can be reduced below the genuine electron background provided that the transverse segmentation of the electromagnetic calorimeter is of the order of $\Delta\eta.\Delta\phi = 0.02^2$. These rejection factors should be compared and contrasted with those obtained by other identification techniques discussed by the Electron Identification Working Group [15].

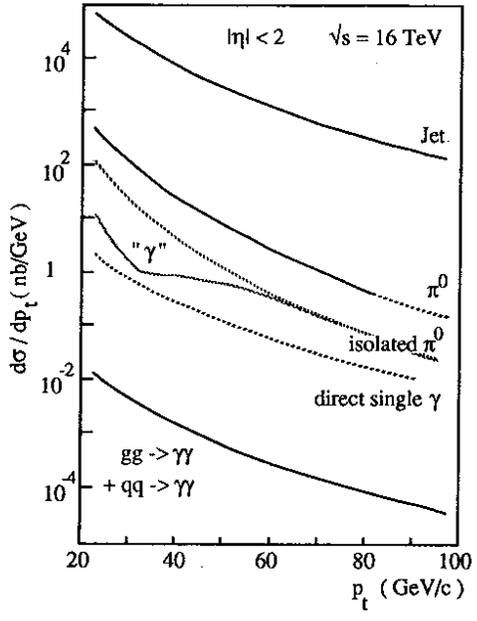

Figure 13 : Inclusive cross-sections for jets, π^0 and direct photons in a rapidity range of |η|=2. The effect of isolation criteria (isolated π^0)[5] is shown together with the additional rejection one could obtain from the observation of the 2 γ's from the π^0 which are separated in angle by ≥ 5 mrad ("γ").

1.6.2 Photon Identification

The process pp -> H -> γγ is a crucial one for the detection of an intermediate mass Higgs boson at the hadron colliders. The irreducible background, from QCD di-photon production, is large and hence very good mass resolution is required for the H -> γγ peak to stand out in the slowly varying background. However the reducible background, from π^0's in jets, would be

dominant unless reduced substantially. Fig 13 shows the inclusive cross-sections for jets and π^0's as a function of p_t in a rapidity range of $|\eta| \leq 2$ [5]. The jet background, surviving the cuts described in 1.5.1, is below the inclusive π^0 spectrum and is dominated by the isolated π^0's. A further rejection factor of ~ 10 is required, especially for π^0's at low p_t, to take the background from two jets, both faking photons, substantially below the direct di-photon background. For such a reduction a calorimeter capable of detecting the presence of two photons having an angular separation of $\geq$ 5 mrad is needed as shown in Fig. 14.

1.7 Calorimeter Resolution

1.7.1 Electron Energy Resolution

Good energy resolution for leptons is essential for the measurement of masses and widths of new, narrow and heavy objects eg. a Z' decaying into a pair of energetic electrons [16]. In such an energy range ($\geq$ 500 GeV) the ability of a calorimeter to measure the energy is limited by the control of the systematics and the knowledge of the energy inter-calibration. With some care 1-2% energy resolution can be achieved (see section 2 below). Such a resolution seems well matched to the natural widths predicted for these new particles by most models. On the other hand, this process defines the large dynamic range required as particles with a mass of up to 4 TeV could be detectable using the high luminosity available at the LHC.

Electromagnetic calorimeter energy resolution is also important in the search for new particles with a Z among the decay products like in the mode H -> Z Z* where both the production cross-section and the Higgs width is small. A powerful tool to extract a signal from a large background is to compare the reconstructed mass of an electron pair to the Z mass. Here a better resolution allows a tighter mass cut resulting in a smaller non-resonant background. However in this particular channel, resolution may not be critical as the background, coming mainly from $t\bar{t}$ -> 4e and Zb$\bar{b}$ -> 4e [17], is not very large and can be further reduced by lepton isolation cuts. Note here that the isolation requirement is also necessary for muons. Indeed, the muon momentum resolution usually is not as good as that for an electron.

1.7.2 Photon Energy Resolution

Photon energy resolution appears to be much more important. The H -> $\gamma\gamma$ channel seems to be the best candidate for the detection of a Higgs if its mass is in the range 80-130 GeV/c^2. As mentioned earlier there is a large irreducible background from QCD prompt photon production. However as the Higgs has a very small natural width in this mass range the signal can be extracted if the $\gamma\gamma$ mass resolution is good enough [5]. Fig 14 shows the statistical significance of a Higgs signal as function of the calorimeter resolution for an integrated luminosity of 10^5 pb^{-1} ($\oplus$ denotes the squareroot of the sum of the squares). A very low sampling fluctuation term typical of homogeneous calorimetry is useful only if the systematics can be kept below $\approx$ 0.5 % .

In addition, all the benefit of very good photon energy resolution is lost if the vertex position is not known to within a certain precision. This leads to a deterioration of the $\gamma\gamma$ mass resolution due to the resulting uncertainty in the angle between the two photons. The calorimeter must thus have some pointing capability with a precision of $\approx$ 5 mrad. Moreover in Fig.14 it is assumed that all isolated π^0 from hard jet fragmentation, with a $\gamma\gamma$ angular separation of $\geq$ 5mrad, have been removed (see 1.6.2). Combining all these properties will certainly be a challenge for the calorimeter builders.

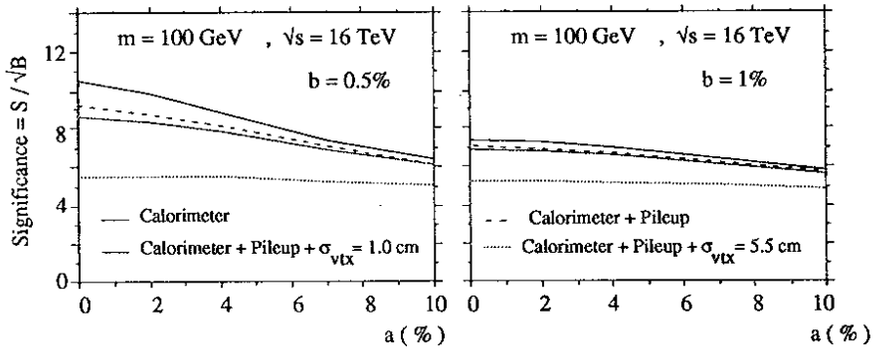

Figure 14 : Significance of a peak in the 2 γ mass distribution as function of the calorimeter resolution parametrized as $a/\sqrt{E} \oplus b$. The effect of pileup and the dependence on the precision of the vertex position is also shown. Only the 2 γ irreducible background is considered. The QCD jets hadronizing into isolated π^0 and faking a γ are assumed to have been removed.

1.7.3 Hadron Energy Resolution

Several reactions have been studied at this workshop to investigate the requirement on jet energy resolution.

It would be advantageous to try detect an intermediate mass Higgs via its abundant H -> b$\bar{b}$ decay mode. The reaction pp -> ZH -> ee + b$\bar{b}$ has been studied [18]. Fig16 shows that the b$\bar{b}$ mass distribution has an r.m.s. width of $\approx$ 11 GeV due to b fragmentation effects alone and would only marginally be further widened by a poor calorimeter resolution of $100\%/\sqrt{E} \oplus 4\%$. It seems to be very difficult to extract this signal from the much more abundant Z+2 jets background. One way out could have been to increase the luminosity in order to improve the statistical significance of the signal. However the multiple event pile-up starts to dominate as discussed in section 1.4. Fig. 17 compares the reconstructed mass distribution, at the particle level, of a Z -> jj decay without pileup and in the presence of 40 minimum bias events. Even when a very small cone half-angle of $\Delta R = 0.3$ is used to measure the jet energy, in order to minimize the pile-up contribution, the r.m.s. of the Z peak is still $\approx$ 12 GeV before any smearing due to calorimeter resolution is taken into account.

An area where one would benefit from the large branching ratio of Z -> jj is the search for the Higgs in the high mass region. Although in this region the Higgs particle has a large width and does not require good mass resolution, one would like to extract the signal by reconstructing the decay Z -> jj. This has been studied for a Higgs boson of a mass of 800 GeV/c^2. The Z's are produced at large transyerse momenta and hence the decay jets start to merge. Hence the jet jet mass resolution turns out to be poor ($\sigma \sim 12$ GeV) even before account is taken of the smearing due to the finite calorimeter energy resolution. The σ increases to only 13.1 GeV if a calorimeter with an energy resolution given by $100\% / \sqrt{E} \oplus 4\%$ is used.

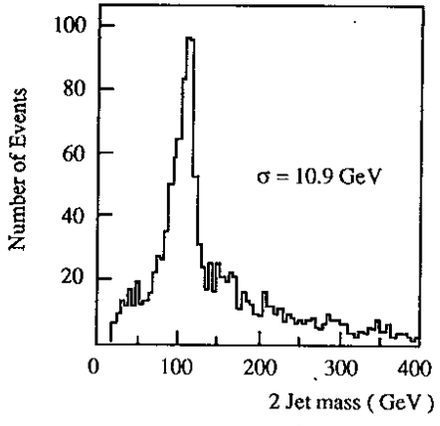

Figure 16 : Two jet mass distribution in the pp -> ZH -> ee + $b\bar{b}$ reaction. Smearing due to finite calorimeter energy resolution is not included.

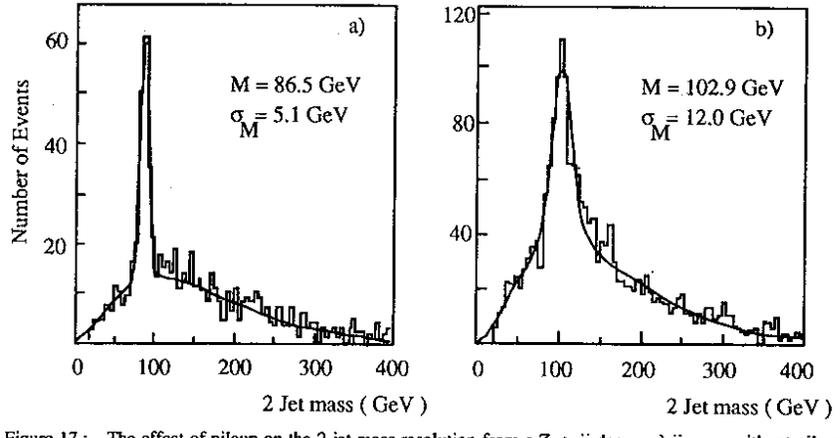

Figure 17 : The effect of pileup on the 2 jet mass resolution from a Z -> jj decay. a) jj mass without pileup; b) in the presence of 40 minimum bias events. Smearing due to finite calorimeter energy resolution is not included.

The reconstruction of the mass of the top quark has been studied [8] using the jets in the reaction pp -> $t\bar{t}$ where one of the two top quarks decays semi leptonically and provides the trigger. The other one decays into 3 jets which are then used to reconstruct the mass. As the cross section for this channel is large it can be studied at a relatively low luminosity. Pile-up is then not a problem. The 3 jet mass distribution is wide and sits on a large combinatorial background. Thus here again the calorimeter resolution does not seem to be critical. It is also interesting to note that the multilepton channel $t\bar{t}$ -> 3 l + X provides a more accurate determination of the top mass [8].

The top working group has also studied the production of the charged Higgs in the decay t -> bH^+, H^+ -> $c\bar{s}$. For some values of the parameters in the minimal SUSY model, the width of H^+ can be small. The bH^+ decay mode competes with the t -> bW^+ one. Fig. 18 shows the mass distribution of two of the three jets. A H^+ signal can be seen close to the W peak. This simulation was carried out using a calorimeter with an energy resolution given by $50\% / \sqrt{E} \oplus 2\%$. The separation of the H^+ peak from the W one becomes marginal in a calorimeter with a worse resolution eg. $100\% / \sqrt{E} \oplus 4\%$.

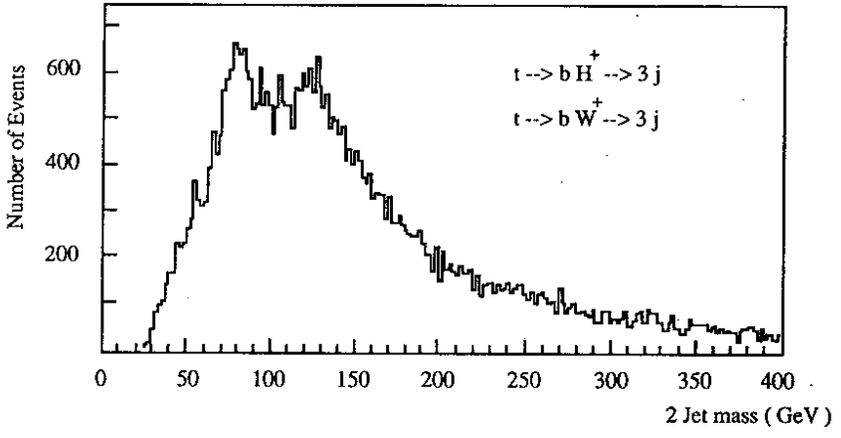

Figure 18 : The mass distribution of two out of the three jets from the decay t -> bH^+, H^+ -> $c\bar{s}$ and t -> bW^+

1.8 Summary : Physics Requirements

This ends the brief survey of physics requirements on calorimetry. The main ones are :

- an ability to stand luminosities in excess of 10^{34} cm^{-2} s^{-1} which implies the need for a radiation hard calorimeter that can provide fast signals.

- Detection and energy measurement of leptons is crucial requiring a calorimeter that can provide the trigger, the identification and a good energy measurement of the electrons. This requires fine lateral segmentation of the electromagnetic part of the calorimeter.

- A geometric acceptance for electrons and photons of at least ± 2, and possibly ± 3, units of rapidity. A useful measurement of the missing transverse momentum and the search for a heavy Higgs via jet tagging requires an even larger rapidity coverage for jets (at least ± 4 units). This is summarized in Fig. 19.

- The requirements on energy resolution are process dependent. The most demanding one is H -> $\gamma\gamma$ for the electromagnetic calorimeter. For jet energy measurement at high luminosity, event pile-up will limit the performance of a good hadron energy resolution calorimeter.

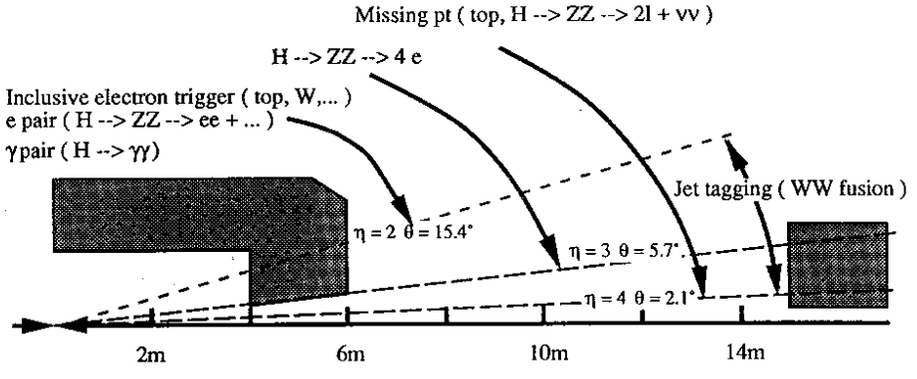

Figure 19 : Angular acceptance requirements from various physics processes.

2. CALORIMETER TECHNIQUES

The most serious problem that all calorimeter techniques will have to solve is the one of radiation damage. To underline the importance of this problem, we discuss it first. Then we report on the various techniques that were reviewed during this Workshop.

2.1 Radiation Levels

The high luminosity needed to study low cross-section phenomena will induce high radiation levels in the calorimeters. This has already been discussed at Barcelona in the previous ECFA meeting by D. Groom and G. Stevenson [2]. Since then, a more detailed computation, using hadronic cascade simulations, has been performed and has confirmed the previous results apart from a change in the value of the hadron and photon dose [19].

The basic assumption is that beam-beam collisions dominate over other sources of irradiation. This is not true at the present proton-antiproton collider but is expected to be so at the LHC in view of the much higher interaction rate. The computation by Stevenson assumes an inelastic interaction cross-section of 60 mb, a 3 m thick spherical lead calorimeter starting at an inner radius of 2m. The computation should be correct to within a factor of 2. Simulation of the eventually chosen geometry will obviously have to be done. However, for this study we have simply scaled the dose and the neutron fluence, at a given angle, by the inverse of the square of the distance from the interaction vertex. This may introduce some additional uncertainties.

Consider a detector running for 10^7 seconds / year at a luminosity of 2.10^{34} $cm^{-2}s^{-1}$ and for 5 years. The doses which the calorimeters will have to stand, under these conditions, is illustrated in Fig. 20 for two typical calorimeter configurations. The dose reaches a maximum in the electromagnetic part of the calorimeter and comes from the myriad of low energy π^0 produced in the pp collisions. The typical dose in the large central barrel is ~10^4 Gy and is four times higher in the compact design. As was already stressed in Barcelona, the situation worsens rapidly when one gets closer to the beam line where a level of ~ 4.10^5 Gy is expected at a rapidity of 3 at a distance of 4m (and ~$1.6\ 10^6$ Gy for the compact calorimeter). In this angular region, the radiation level increases by ≈ 20 per unit of rapidity and the forward calorimeter, even if it is retracted as far back as 15m from the interaction region, will have to stand more than a MGy.

Damage may depend on the type of irradiation eg. silicon detectors are much more sensitive to low energy protons and neutrons (see 2.6 below). The neutron flux is also large ranging from 10^{14} n/cm^2 in the barrel region to more than 10^{16} n/cm^2 in the forward region (Fig. 20). The energy spectrum of these neutrons peaks around 1 MeV. The exact neutron flux depends on the precise calorimeter composition. If uranium is used as absorber, instead of lead, the neutron flux increases by ≈ 2. If iron is used, the neutron flux decreases by ≈ 2.5. The presence of hydrogenous materials like scintillators decreases the flux by ≈ 3.

Under this large irradiation, the calorimeter itself will become radioactive. This is especially true for calorimeters in the forward region where the induced radioactivity will be in the range of

milli Sievert per hour. The materials will have to be carefully chosen to minimize activation, and from this point of view, uranium does not seem to be the best choice. For more details the reader is referred to the report by G. Stevenson at this workshop [19].

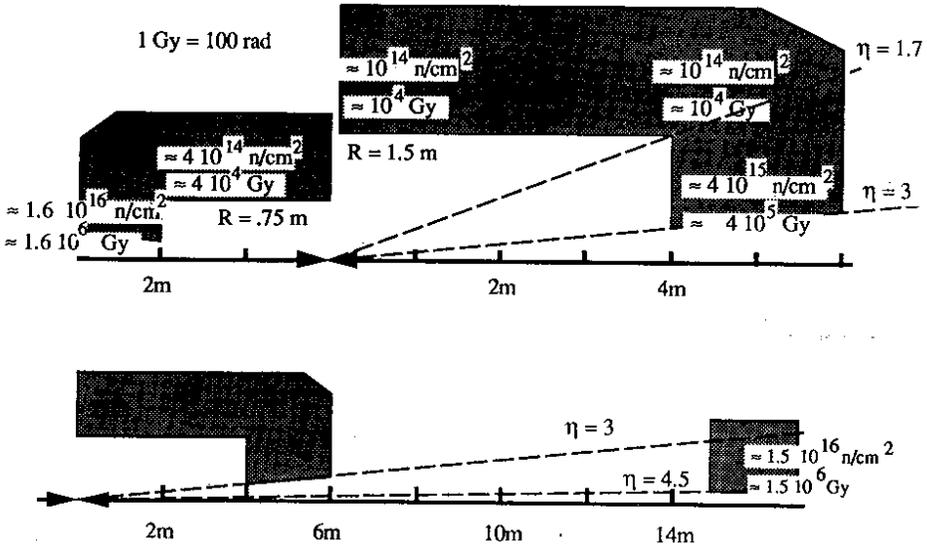

Figure 20 : Typical doses and neutron fluences in a calorimeter exposed to an integrated luminosity of 10^{42} cm^{-2}.

2.2 Scintillator Tiles-Wavelength Shifter

The technique of scintillator (SCI) tiles read-out via wavelength shifter (WLS) plates, rods or fibers has been used in numerous sampling calorimeters. After the pioneering work of the AFS Collaboration [20], the ZEUS collaboration [21], through a systematic programme of tests, have optimized this technique as far as energy resolution for hadrons and jets, compensation, calibration and uniformity are concerned. The main achievements are (Fig. 21) :

- hadronic energy resolution : 35% / $\sqrt{E}$ with a constant term <1% and a noise of 180 MeV for a calorimeter volume of 1 m^2 x 7 interaction lengths,
- an electron energy resolution: 18% /$\sqrt{E}$ with a constant term <1% and a noise of 8 MeV for towers containing electromagnetic showers,
- e/h=1 to within 2% for energies above 2 GeV,
- tower to tower calibration of ≈ 1% using the uranium signal (thus avoiding the need to calibrate in particle beams) ; a similar number is expected for the absolute energy calibration,
- transverse uniformity for electrons within a tower of ≈ 2%,

- spatial (lateral) uniformity for electrons between modules of ≈ 5% (for angles between the incident particle and the module boundary above 40 mrad),
- spatial (lateral) uniformity for hadrons ≈ 2%,
- timing accuracy of ≈ 1 ns for signals above a few GeV.

It was mainly through the experimental and theoretical work on U/SCI and Pb/SCI calorimeters, that the present understanding of compensating hadron calorimetry has been reached. As a result detailed experimental data and simulation programs are readily available both of which are very useful for any calorimeter design and optimization.

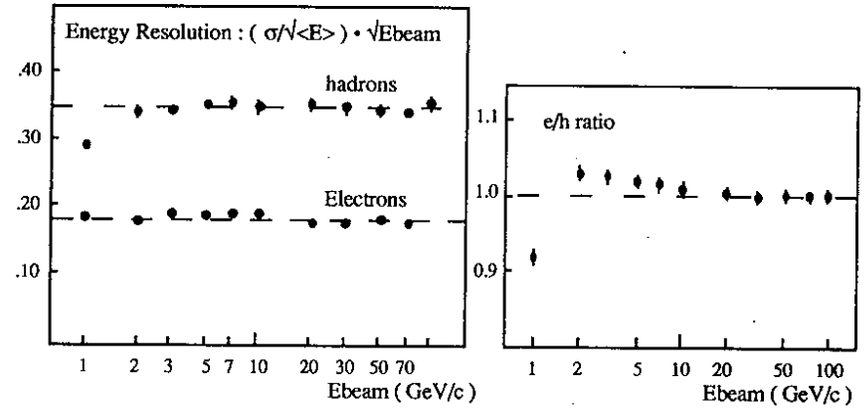

Figure 21 ZEUS prototype calorimeter : a) energy resolution for electrons and hadrons, and b) the e/h ratio.

The strength of this technique lies in the excellent energy resolution for hadrons, in particular at high energies, that can be achieved if the correct material thicknesses are chosen, the low energy equivalent of the noise and the vast amount of experience. If uranium is used, its radioactivity provides an excellent calibration signal. The problem of the uniformity of response between the modules has been solved by placing lead absorbers between the modules. These absorb some of the shower energy to counterbalance the Cerenkov light produced in the WLS's. The use of plastic SCI and photomultipliers results in fast signals with a typical decay time constant of ~10 ns. There is an additional tail arising from the time taken for the neutrons to be moderated in the SCI. These are the neutrons that provide the necessary "nuclear signal" to achieve compensation. This signal is also fast and has essentially died out after 40ns. Such integration times however are required for perfect compensation. For a discussion of the time dependence of the signal we refer to [22]. Given the fast pulses and the low noise, timing resolution below 1 ns can be achieved. Thus an assignment of a signal to the proper bunch crossing is relatively easy, as is the detection of off-bunch pileup.

The drawbacks of compensating calorimeters readout via SCI tiles and WLS are :

- the limited electromagnetic energy resolution,
- the limited segmentation, both longitudinally and transversely and

- the difficulty in achieving projective geometry.

Experience in ZEUS suggests that a transverse segmentation better than 5cm x 20cm (with readout on two sides over the 20cm) will be difficult to achieve. This can be partially compensated for by the installation of finely segmented position detectors in the front part of the electromagnetic section (eg. ZEUS use silicon pads [23]). By placing these detector planes, having a segmentation of 10 square centimeters, at a depth of 3 and 6 radiation lengths, they achieve a hadron rejection of ≥200 for an electron efficiency of 90% for particle energies ≥ 10 GeV. Their segmentation is too coarse to achieve a position resolution beyond the pad size. A finer segmentation can clearly result in an improved hadron rejection, a more precise determination of the shower position and the angle of photons and a better separation of nearby showers.

To improve the segmentation, SCI both liquid and solid, can be readout using WLS-fibers. This has been done by several groups in the past (eg. MPI-Munich, UA1-tests, ZEUS-tests [24 a,b,c] respectively), and was again presented at this workshop [25]. It is also one of the options for calorimetry in the SSC detectors. Progress has been made at Serpukhov by embedding the WLS-fibers into plastic SCI at the SCI production step via injection molding and by developing a technique of efficient and reproducible coupling of WLS-fibres to clear fibres. However no new experimental results on the uniformity, which has been one of the reasons why this technique has not been used in large experiments, have been shown. Another difficulty of this design is the enormous number of fragile fibers which have to be handled.

For an LHC calorimeter the radiation damage of SCI and WLS is the major concern. ZEUS have made a detailed investigation of the radiation sensitivity of their SCI (SCSN-38) and WLS (Y7 dissolved in PMMA) [26]. Both materials show a very strong reduction in attenuation length immediately after irradiation at a high dose rate (above 100 Gy/h). In the presence of oxygen (eg. air), the material recovers within days for SCSN-38 and ~ 1 year for Y7-PMMA with some sign of permanent damage. In an experiment an equilibrium of damage and recovery close to the level of the permanent damage will be reached. Radiation damage also causes a decrease of the local light yield of about 4% / kGy in both air and nitrogen. Taking as a criterion that an acceptable dose only results in :

i) a deterioration of $\leq \pm 2\%$ in the uniformity (lateral) of response over a cell size of 20 cm read out from two opposite sides,
ii) a longitudinal uniformity for the WLS's of $\leq \pm 5$ % in the electromagnetic section of a depth of 25cm and
iii) a longitudinal uniformity of $\leq \pm 10\%$ in the hadronic section of a depth of 60cm

a calorimeter like the one of ZEUS could work up to integrated doses of ~10-20 kGy. From the recent progress in radiation resistance of SCI-fibers [27] one can expect an improvement of a factor ten in radiation resistance over the next few years. Thus it may be possible to use this technique up to a rapidity of about 2.5 at the LHC.

Compensation requires a SCI/U volume ratio of about 0.82. This volume ratio is ~ 0.25 for SCI/Pb. This requires thin SCI plates, especially for Pb, in order to achieve an electromagnetic resolution of 15% / $\sqrt{E}$ or below. This results in a light yield which is marginal if

photomultipliers are used as these typically have quantum efficiencies of ~15%. An improvement in the light yield (eg. optical cladding of SCI or WLS to improve the light transport, more efficient SCI or more efficient photodetectors etc) would be very desirable.

Photomultipliers (PMs) are normally used to read out compensating SCI/WLS calorimeters as solid state photodiodes are too noisy given the small light yield (≈ 200-500 photoelectrons/GeV for PMs). It appears that the gain and resolution of PM's with synthetic quartz windows is not affected by doses up to 4.10^5 Gy and 4.10^{14} n/cm^2 [28]. PMs with linear dynode chains have a typical lifespan of 500 to 1000 C of charge seen by the anode, and thus will have to work at low gain at the LHC. Another reason to work at low gain is the dependence of the gain on the anode current (typically 0.5% / μA). PM's may have the required dynamic range for experimentation at the LHC as ZEUS already use signals from 1 to 80,000 photoelectrons. The gain of PM's, even of the mesh type, is affected by magnetic fields, and different photodetectors would have to be developed if the calorimeter is required to work in a strong magnetic field. The light yield of plastic scintillators also depends on the magnetic field.

G.Stevenson [19] has pointed out that the use of uranium as the absorber in a LHC calorimeter is very undesirable because of the increased neutron production and the secondary activation - this has to be checked quantitatively. However without uranium radioactivity it may be difficult to achieve the ≤ 1% calibration accuracy for an optical detector in the LHC environment. Secondary activation in the high radiation field at LHC also rules out the use of the uranium radioactivity as a long term calibration method. Thus lead may be a more suitable absorber material.

Large calorimeters based on SCI tiles have already been built and an extension to the dimensions required at the LHC appears reasonable, but no work towards this goal has yet been done. The difficulty in realizing a projective geometry should be kept in mind. Because of the coarse segmentation and energy resolution, this type of calorimeter does not fulfill the requirements of electromagnetic calorimetry at the LHC. It may offer an attractive and economic solution for a compensating hadron calorimeter following a high resolution electromagnetic calorimeter. However there are a number of problems that have to be resolved before an LHC calorimeter can be built. At present the necessary R&D is not being pursued.

2.3 Scintillating Fibers

To overcome the drawbacks of the SCI-WLS technique while retaining its advantages, calorimeters using scintillating fibers are being developed. The most impressive results so far have been shown by the SPACAL collaboration [29]. They use 1 mm diameter SCSN-38 plastic fibres, embedded in a Pb-matrix, which run at a small angle with respect to the direction of the incident particles. The SCI/Pb volume ratio is chosen to be 0.25 to achieve compensation. This results in a very dense calorimeter having a short radiation (0.75cm) and interaction (21cm) lengths. A fine lateral granularity and an excellent uniformity of response can be achieved without the introduction of dead spaces. Given the small intrinsic fluctuations

of about 12% /√E for a compensating SCI-Pb calorimeter [30], a hadronic energy resolution of ~ 30%/√E + ≤ 1% is expected and an electromagnetic energy resolution of ~13% / √E + 1% has been measured. The SPACAL group has addressed most of the problems eg. fiber to fiber uniformity, uniformity along the fiber, optical readout, embedding of the fibers into the lead matrix, radiation damage etc. and have built a series of prototype calorimeters, the largest one with a diameter of 1 m and a depth of 10 interaction lengths. The progress and the results obtained in a recent beam test are impressive (Fig.22) :

- energy resolution for electrons of 13% /√E+ 1% for incidence angles greater than 50 mrad (at lower incidence angles a non Gaussian tail towards higher pulse heights develops due to the channeling of particles in the fibers),
- position resolution for electrons of 1.8 mm at 80 GeV for a readout segmentation of 48.7 cm^2,
- uniformity of response to electrons of 1% even over tower boundaries,
- e/π measured to be ~ 1.05,
- hadronic energy resolution of 30% / √E + 2.6%, with a small non-Gaussian tail towards higher pulse heights,
- hadron jet resolution better than the hadronic energy resolution, measured by using interactions in a CH target placed in front of the calorimeter,
- position resolution for hadrons of 5.0 mm at 150GeV for a readout segmentation of 48.7 cm^2,
- a fast pulse shape. After unfolding the effect of the cable a FWHM of 4 ns for electrons and 6.4 ns for hadrons, with a tail of 10 ns time constant from the moderation of the neutrons is observed [11].
- hadron (isolated) rejection of 800 at 99% electron efficiency from the analysis of pulse shape.

In addition the group has presented results on the time dependence of e/π and on the influence of the transverse containment on the hadronic energy resolution.

Work is in progress to understand and improve the hadronic energy resolution, where the optimum value has not yet been achieved. The main difficulty is due to the remaining longitudinal non-uniformity of the fibers. The response increases by about 30% in the last 30 cm near the readout device. This results in the non-Gaussian tail in the hadronic energy resolution for the showers that develop late (Fig. 22 a). If these showers can be identified, a correction can be applied and the hadronic energy resolution at 150 GeV improves from 4.8% to 3.7%. This effect is significantly reduced for jets, which are typically one interaction length shorter than single hadron showers of the same energy and also exhibit smaller longitudinal fluctuations.

The longitudinal non-uniformity of the readout also reduces the measured e/π ratio. It is estimated that the corrected e/π should be about 1.1 for the present prototype. The hadron response is about 10% smaller than expected, presumably due to the proton recoil energy lost in the cladding of the fibers.

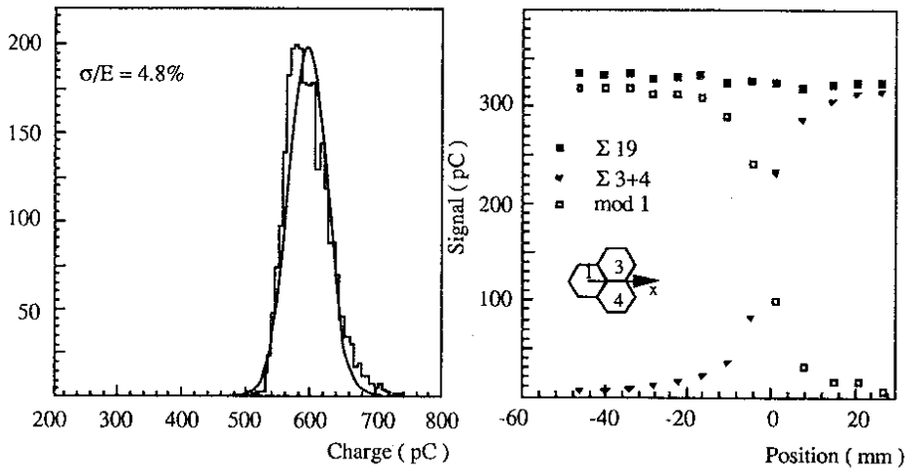

Figure 22: SPACAL test : Energy response for 150 GeV/c pions and uniformity scan for 80 GeV/c electrons at modules boundaries.

Again it is the radiation damage of the SCI fibres which is the major worry for an LHC detector. This is particularly difficult because of the length of the fibers and the sensitivity of the response to longitudinal non-uniformities. The non-uniform distribution of the radiation dose (maximum in the electromagnetic section) eases the problem somewhat as has been shown by a Monte Carlo study by the SPACAL group [27]. A major R&D effort on the evaluation and improvement of radiation resistance of plastic scintillation fibers by several groups has already shown encouraging results. For details we refer to the working group on radiation damage. Results on new fiber compositions (eg. 3HF doped with PTP) have been shown. 38cm long fibres have been irradiated up to 220kGy and the maximum light losses have not exceeded 50%. It is hoped that eventually radiation hardness up to 100 kGy can be achieved, so that the coverage up to rapidities of 2.5 could be reached at the LHC.

Calibration at the 1% level is very difficult particularly for techniques using optical readout. No new ideas on how this can be achieved have been presented at this meeting. It is felt that a systematic R&D on this question is required before building an LHC calorimeter.

Present prototypes are read out with PM's and the comments made in section 2.2 apply. To fully exploit the high transverse granularity a more segmented photodetector is desirable. The quite old idea of the hybrid vacuum photomultiplier (photocathode, a high drift field with about 10kV potential difference and a silicon detector to detect the accelerated electrons) has been revived and prototype samples have been produced by industry though no quantitative results have yet been shown. As this readout technique (assuming it will stand the radiation dose at the back of the calorimeter) is very promising for other applications as well, its R&D should be pursued.

There was a lot of discussion about the need for longitudinal segmentation. In the design of a projective calorimeter of the SPACAL type some longitudinal segmentation is achievable as only a fraction of the fibers will start at the front face. Thus grouping of the readout will give some longitudinal information. The extent to which electrons can be identified and measured in the midst of jet fragments at high luminosities with the SPACAL segmentation is under study.

First sketches of a projective SPACAL calorimeter for the LHC have been shown. A possible layout can also be found in the expression of interest of the TEXAS SSC detector. So far no practical solution for the construction of a self supporting Pb/fiber structure has been presented and R&D work should focus on this issue. The manufacture of the enormous number of fibers within strict quality criteria needs a major breakthrough in the production and the quality control techniques to make such a calorimeter affordable.

To summarize, compensating fiber calorimeters are good candidates for high resolution hadronic calorimeters at the LHC, in particular in a limited central rapidity range. There is however a number of difficult questions to be solved before a LHC calorimeter can be built.

2.4 Liquid Argon

Major progress has recently been made in the field of liquid argon sampling calorimetry in spite of it being a mature technique and in use for many years.

- The H1 collaboration has built a hermetic electron/hadron calorimeter with a large solid angle coverage for HERA and have shown that given a fine longitudinal granularity weighting methods can achieve a hadronic energy resolution of $44\% / \sqrt{E} \oplus 1\%$. Even better energy resolution and a linearity within 0.5% are achieved for jets [31] (Fig.23),
- the Helios collaboration at CERN has operated a liquid argon uranium calorimeter with a peaking time of ~150 ns, with preamplifiers immersed in the liquid,
- a new readout geometry, named the "accordion" (Fig 24), has been designed and recently tested at CERN leading to a realistic hope of achieving peaking times around 40 ns with an electronic noise level equivalent to ~200 MeV for electromagnetic showers [32].

In addition, the known strengths of liquid argon sampling calorimeters are :

- temporal stability and calibration,
- (probable) radiation resistance up to doses of more than 100kGy (limited by the readout electronics),
- readout uniformity,
- flexible granularity, making possible the construction of calorimeters with good spatial resolution, electron /hadron separation etc... ,
- possibility of achieving an electromagnetic energy resolution of $8\% / \sqrt{E}$ with a constant term below 1%.
- insensitivity to magnetic field.

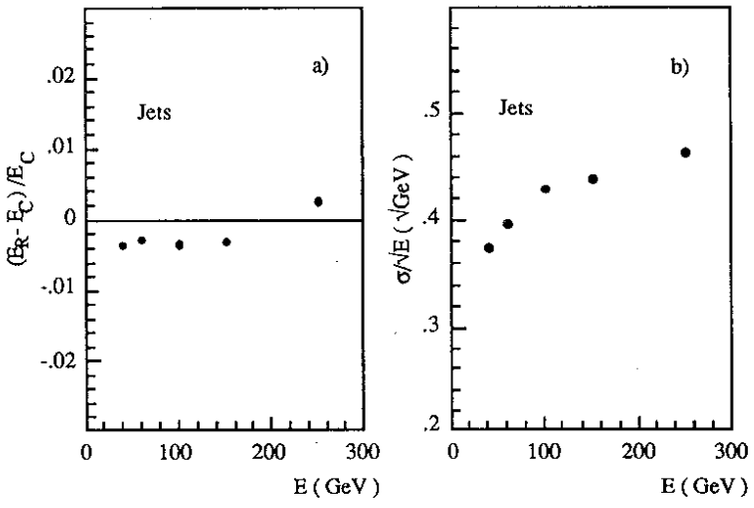

Figure 23 : H1 test : Linearity of jet response and the energy resolution for jets using the H1 weighting algorithm.

The main difficulties of this technique are:

- the speed of the charge collection and the charge transfer to the electronics,
- moderate hadronic resolution of $50\% / \sqrt{E} + 3\%$, unless a weighting technique is used,
- the need for a cryostat, which makes a hermetic design difficult, and which introduces about 0.5 - 1.0 radiation length of material in front of the active part of the calorimeter.

For a description of the accordion layout we refer to [32]. To avoid channeling absorber plates and readout gaps are shaped as in an accordion (Fig.24). The readout boards are made from multilayer Kapton foils with resistive coating, thus already including the blocking capacitors. The preamplifiers are directly connected to the Kapton boards, thus minimizing the capacitance and the inductance. This results in about a factor of five reduction in the capacitance per unit volume compared to the already optimized Helios layout. The preamplifiers are immersed directly into liquid argon. A prototype that can contain high energy electromagnetic showers has been built with a total of 16 x 15 cells of dimensions of 2.5 cm x 2.7 cm each. There are two longitudinal readout segments, with the amplifiers placed at the front (for the first sampling) and at the rear (second sampling) of the calorimeter. Si J-FET's and GaAs MESFET's were used, together with the Helios shapers having a peaking time of 140ns. The main results (preliminary) obtained so far are:

- a noise equivalent to ~ 25 MeV for towers containing a high energy electromagnetic shower, with negligible coherent pickup,
- an electromagnetic energy resolution of $10\% / \sqrt{E} + (0.03 \pm 0.05)\%$,
- lateral uniformity of response within 1%,

- linearity of response within 1%,
- position resolution of ~ 0.5mm in both the directions for 125 GeV electron showers,
- measurement of the shower direction with a precision of ~ 7 mrad at 100 GeV.

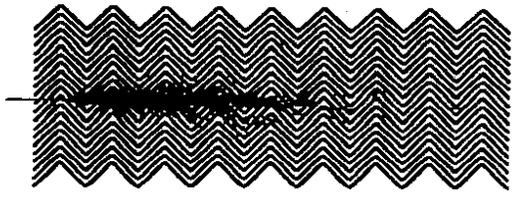

Figure 24 : A 40 GeV electron showering in a lead liquid argon accordion structure. The lead absorber plates run at ± 45° to the particle direction thus avoiding channelling. Preamplifiers are located at the front and at the back of the calorimeter, minimizing the connection capacitances.

Further beam tests are planned for spring 1991 using electronics with a peaking time of 40 ns. As a next step towards an LHC calorimeter the following R&D has started:

- design to be followed by the construction of the electromagnetic and the hadronic calorimeter modules with a pointing geometry,
- optimization of the performance by detailed simulation,
- development of appropriate front end electronics,
- development of radiation hard components,
- radiation hardness tests.

For the hadronic sections, where the segmentation will be much coarser (eg. 20 cm x 20 cm) than in the electromagnetic ones, readout pads will be connected in series to improve the impedance matching to the front end electronics. This will result in approximately the same capacitance (400pF) per readout channel as in the electromagnetic part. A detailed simulation study (cross checked with an electrostatic model) indicates that no significant degradation of the energy and position resolution of jets is induced by the effect of de-localisation of charge inherent in such a scheme [33].

Low electron drift velocity and limited hadron energy resolution are drawbacks of this technique. The impact of the low drift velocity on pileup can be minimized by bipolar shaping. So far excellent hadronic energy resolution, at high energies, has only been achieved via software compensation. One idea to improve the e/h is to reduce the electromagnetic response by cladding a high Z (eg. Pb) absorber material with a low Z material (eg. Fe) to stop the low energy electrons penetrating into the active part of the calorimeter. This is presently under study, but from the experience of the ZEUS group, who have a foil of 0.4 mm of Fe separating the U absorber and the plastic scintillator, the maximum reduction of e/mip is only about 4% and thus not sufficient to achieve compensation.

Dopants may be used to increase the signal from heavily ionizing particles and possibly increase the electron drift velocity at the same time. One of the difficulties of doping will be to achieve both a stable calibration and radiation hardness.

Several groups have studied the addition of methane which, in a concentration of about 0.5%, doubles the electron drift velocity in liquid argon. At the same time the recoil protons, from neutron interactions, may boost the hadron signal. Experimental studies by Helios and others observe the increase in speed, but also observe a worsening of the e/h ratio from 1.1 to 1.15 at 100 GeV, due to the increased charge saturation for highly ionizing particles.

The e/h ratio may be improved by using a photoionizing additive to transform the UV scintillation light from LAr, which shows no ionization saturation, into charge. As LAr emits two components with time constants of 6 ns and 1000 ns, the slow component has first to be quenched. This can be done with 125 ppm LXe, resulting in a decay constant of 65 ns, or by LN_2 leading to a decay constant of 5.6 ns. There are many candidates for photosensitive dopants, eg. allene (C_3H_4) with a concentration of a few tens of ppms. There are several encouraging lab results and a systematic R&D to investigate the above questions has been started at CERN [34]. It should give first results on performance and also radiation sensitivity during the next year.

To summarize, LAr appears to be one of the prime candidates for use at the LHC with a possibility of providing a large rapidity coverage. A vigorous and systematic R&D program is under way in Europe and elsewhere.

2.5 Room Temperature Liquids

Calorimeters using room temperature liquids [35] attempt to improve on the following drawbacks of liquid Argon:

- slow drift speed,
- limited hadronic energy resolution,
- need of a cryostat.

So far the use of room temperature liquid calorimeters is limited. The two liquids used so far are TMSi and TMP. The UA1 collaboration has built and tested a U-TMP calorimeter with a depth of 2.35 interaction lengths followed by a Fe-SCI backing calorimeter [14]. The uranium calorimeter consists of an electromagnetic part made out of 2 mm U-plates, split into 4 longitudinal samplings, and a hadronic one made out of 5 mm U plates and split into two sections. A position detector (filled with TMP) is placed at 3.5 radiation lengths. The TMP is contained in stainless steel boxes of a thickness of 3.3 mm. At a field of 12 kV/cm the charge collection time is ~ 300 ns. A 1μs shaping time is used and the equivalent noise is ~ 100 MeV for a high energy electromagnetic shower and ~ 1 GeV for hadron showers. The measured resolution for electrons is $12\% / \sqrt{E} \oplus \leq 1\%$. For hadrons it is $58\% / \sqrt{E} \oplus 6.8\%$ (Fig.25). The method used to extract the e/π ratio, quoted to be about 1.05, introduces some effective weighting. The tower to tower uniformity is better than 1%. The frames of the ionization chambers are made from stainless steel bars of a width of 3 mm resulting in a drop of ~60% in the electron response where the two ionization chambers meet. No change in the free electron

lifetime in a prototype electromagnetic calorimeter, initially measured to be ~ 15μs, has been observed over the last 4 years. Lifetimes of several hundred μs are routinely achieved in the purification but only a lower limit of ~ 30μs can be obtained for the liquid in the ionization chambers. The position detector (PD), which consists of strips with a pitch of 9.1 mm, achieves a position resolution of ≤ 1 mm for electrons with an energy ≥ 30 GeV. A hadron rejection factor of ~10,000 is achieved using the full lateral and longitudinal segmentation of the calorimeter and the position detector for an electron efficiency of 90% .

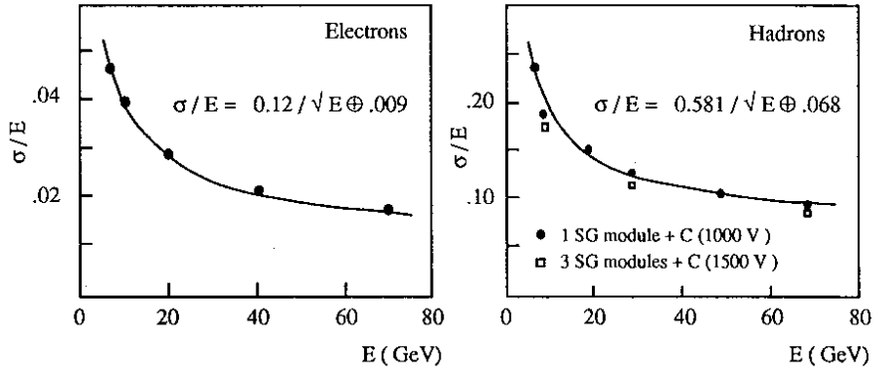

Figure 25 : UA1 uranium-TMP test : energy resolution for electrons and hadrons.

The WALIC Collaboration is also conducting tests using TMP [36]. They are building a modular calorimeter consisting of 70 planes (60 x 60 cm^2) of TMP filled ionization chambers of a construction similar to the ones used by UA1. These can be interleaved with absorber plates made out of different materials. First tests were done at FNAL this summer using 34 TMP chambers. An energy resolution for electrons of 18% / √E with a constant term of 2.7%, attributed to the beam momentum uncertainty, has been measured using absorber plates of a thickness of 6.35 mm of Pb. The electronics noise was ~150 MeV. For the hadronic setup, only shower profiles have been shown.

An ITEP / Karlsruhe collaboration [37] is preparing a modular test calorimeter with 100 TMSi chambers and U, Pb, Cu and Fe as absorbers. Presently 40 planes are available and measurements done at ITEP using a single plane placed at different positions in the calorimeter for various absorber combinations have been presented.

As a result of the above systematic test program the calorimetric properties like e/h, hadronic energy resolution, intrinsic fluctuations etc of TMSi and TMP in conjunction with different absorbers should be known soon.

An issue for discussion is whether it is preferable to use room temperature liquids in chambers or to immerse the absorber in the liquid. So far the sealed chamber solutions presented have significant wall thicknesses, resulting in non-uniformities for electrons which are unacceptable for precision calorimetry. An interesting concept [38] uses a welded structure made from the

plastic VECTRA, with metallized electrodes deposited onto the plastic, with thin detection gaps through which the liquid can flow. The absorber pieces are introduced into the VECTRA drawers. The entire structure can probably be baked out before filling. No results have yet been presented.

A study of the compatibility of different materials (W, Ti, Pb, Cu, glue, Kapton) and TMSi, as far as the electron life time is concerned has been presented [38]. It concludes that the materials that do not contain electronegative substances are usually compatible with the room temperature liquids if properly cleaned.

The performance of room temperature liquids under irradiation is one of the major concerns for use at the LHC. Under irradiation radicals are formed, which then interact with the liquid or themselves to produce new compounds. At a dose of 100 kGy typically 1% of the liquid will be destroyed. This can lead to a very large pressure increase and to a reduction in the electron lifetime. In addition positively charged heavy compounds may form insulating layers. Very little is known and a systematic R&D on pressure buildup, life time and analysis of the radiolysis products is planned at CERN. Equally important is the study of the radiation hardness and possible influence under irradiation of the materials in contact with the liquids.

In order to reach collection times comparable to the 15 ns bunch crossing time, much higher field strengths or the use of liquids like TMSi, which is about three times faster than TMP, have to be used provided the safety aspects can be handled. Substantial R&D work on this topic has been proposed [39]. Work is also going on to reduce the time required to transfer the charge to the electronics. As in the case of liquid argon the electrostatic transformer concept (serial connection of the readout gaps) and front end transistors directly mounted onto the electrodes are under study.

To summarize, room temperature liquids are an interesting option for LHC calorimeters. So far it is not yet a mature technology, and a large R&D effort is required to answer all the questions needed before a decision can be made on its suitability at the LHC.

2.6 Silicon Calorimeters

So far the use of silicon diode ionization detectors as a sampling medium in calorimeters has been limited to very specific tasks, like measurement of the luminosity at LEP, the forward plug calorimeter of the H1 experiment or as sampling planes to discriminate hadrons from electrons in the ZEUS calorimeter. There are however several R&D programs underway for electromagnetic and hadronic calorimetry, which have already produced significant results [40].

Potentially silicon as the detecting medium in a sampling calorimeter has the following advantages :

- high speed with charge collection times below 20 ns,
- ease of calibration,
- linearity over a very wide energy range,

- high longitudinal and transverse segmentation,
- compactness, with a typical sampling layer of 0.4 mm,
- insensitivity to magnetic fields,
- room temperature and modest operating voltage (100V).

This should be contrasted to the (present) difficulties:

- lack of radiation hardness,
- high cost of the detectors,
- large number of costly readout channels, if the speed and segmentation offered by silicon is to be properly exploited,
- no large scale experience in experiments,
- no detailed knowledge of the performance for hadron calorimeters,
- uncertainty in simulation due to the small sampling fraction.

The energy resolution for electromagnetic calorimeters using silicon is similar to other sampling calorimeters : 18% / $\sqrt{E}$ for one radiation length sampling with a negligible constant term. The work by the SICAPO collaboration and by a Hamburg/ITEP collaboration shows that the e/mip (mip = minimum ionizing particle) sampling fraction ratio can be tuned by putting low Z materials like G10 or Fe between the high Z absorber (Pb,U) and the Si detectors. Thus low energy electrons, abundantly produced in the high Z absorber due to the strong Z dependence of photo- and Compton-effect, do not reach the detectors. In this way e/mip can be tuned to lie between 0.9 and 0.6. Highly ionizing particles show no pulse height saturation. It thus appears possible to achieve e/h=1. This has been shown by the SICAPO collaboration using 25mm U plates separated by 2mm of G10 from the silicon detectors. Even if compensation is achieved, the expected intrinsic resolution is however worse than the one measured for Pb or U-scintillator calorimeters. This is under study by the SICAPO collaboration, but no data have yet been presented.

Detailed information on the transverse and longitudinal shape of hadron showers has been measured by SICAPO and also by ITEP/Hamburg group. This is used to tune the simulation programs.

The radiation damage of the silicon detectors is under study by several groups. Three effects are important [41] :

- increase in leakage current,
- loss of collected charge,
- change of bulk resistivity.

The damage constants, taking into account the benefits of self-annealing, for the increase in the leakage currents for neutron, hadron and electron irradiation are now well known. Typical values for a thickness of 300 μm are:

- 10 μA/cm^2 per 10^{13} n/cm^2 for neutrons of 1.2 MeV ,
- 10 μA/cm^2 per 10 kGy for protons of 21 MeV,
- 10 μA/cm^2 per 5 MGy for electrons of 2 MeV.

The neutron damage is the most serious. Higher neutron energies cause a damage that is larger by about a factor of two. As the leakage current decreases by about a factor of two for every 8-10°C drop in temperature, cooling the detector may solve this problem.

The charge collection for detectors irradiated with neutrons has been measured separately for electrons and holes. For a flux of 2.4 10^{12} n/cm^2 of 5 MeV typical losses are 1.1% for a 50ns shaping. Self annealing reduces this loss by a factor two in 152 days. Further work on this question, in particular the extension to higher fluxes and the effects of temperature has to be done before firm conclusions can be drawn.

Irradiation with neutrons leads to an increase in bulk resistivity and finally to an inversion from n- to p-type at fluxes around 10^{13} n/cm^2. This has been clearly demonstrated by the Hamburg group. Nevertheless the detectors continued to work without any additional current contribution from the rectifying junction. Apparently the metallisation of the back contact acts as new barrier. More work, including the temperature behaviour is needed.

Significant progress has been achieved on the characterisation of the defects using the DLTS-method. This work leads to a detailed understanding of the damage problems and may give clues how, eg. via specific impurities diffused into the crystals, radiation hard detectors could be built. This interesting possibility will certainly require a lot of development effort and time, and may come too late for the LHC but given its importance, also for other silicon devices like photodiodes, a very strong R&D effort should be supported.

To summarize, silicon detectors for LHC calorimetry, in spite of the many attractive features, have many open questions, and it appears improbable that they will be solved in time for a first generation LHC detector.

2.7 Homogeneous Electromagnetic Calorimeters

The often quoted reason for requiring very high electromagnetic energy resolution is the detection of the Higgs boson in the mass range $80 \leq M_H \leq 150$ GeV/c^2 through its two photon decay mode. As mentioned earlier (sections 1.4.2, 1.6.2), in order to be confident of detecting the Higgs boson at the LHC, in the mass range $80 \leq M_H \leq 130$ GeV/c^2, some further severe constraints are put on high energy resolution calorimeters. These are :

- minimum constant term in the energy resolution. For the above mentioned process a constant term of 0.5% is equivalent to a term ~ 3-4% / $\sqrt{E}$.
- separation of two photons with an angular separation ≥ 5 mrad.
- measurement of the direction of the photons to within ~ 5 mrad.

Homogeneous calorimeters are good candidates to achieve high energy resolution. Such calorimeters cannot be placed very close to the interaction point as explained in 1.4.2. Media with smaller Molière radii can be brought closer but the two photon separation will become correspondingly more difficult. A realistic simulation must be carried out to fix the optimal radius for a given material.

With these conditions in mind we proceed to consider some candidates for very high energy resolution electromagnetic calorimetry.

2.8 Crystals

Several large scale crystal calorimeters have been built in the past eg. Crystal Ball using NaI(Tl), CLEO and Crystal Barrel using CsI(Tl) and L3 using BGO. These have provided valuable working experience of the problems of light collection non-uniformity, monitoring and inter-calibration of crystals together with those related to the mechanical structures. A very high energy resolution of $\sigma/E \sim 2\%/\sqrt{E} \oplus 0.5\%$ has been achieved for a large number of BGO crystals in a test beam. This has yet to be achieved in the running experiment where the resolution for electrons from Bhabba events is presently ~1.3%. This is thought to be due to an uncertainty in the knowledge of the temperature of the crystals indicating the difficulty of achieving small constant terms in large scale structures.

Several crystals fulfill many of the requirements for use at LHC (Table. 2) :

- high speed with very short decay constants for the scintillation light ,
- very good energy resolution,
- large light yield,
- high transverse segmentation,
- short radiation length and Molière radius,
- room temperature operation.

This should be contrasted with difficulties :

- possible lack of radiation hardness of large crystals,
- non-uniformity of light collection,
- high cost of crystals and their readout,
- existence of long decay constants for a major fraction of the light in some cases,
- temperature dependence of the light output in some cases,
- difficulty in obtaining longitudinal segmentation and good two gamma separation,
- possible mechanical brittleness and hygroscopicity,
- problem of readout in a magnetic field if amplification is required in the photo-device.

Radiation hardness tests of crystals are usually made on small samples (~ few cm^3) and with γ or β sources. The intrinsic scintillation process does not appear to be affected even up to doses of 10^7 Gy. However reduced transmission is observed due to the formation of colour centres. This is thought to be due to impurity atoms which are embedded in the crystal lattice. Long crystals are required for good energy resolution but the impurity levels in long crystals increase with increasing depth due to the manufacturing process. Hence long crystals tend to have less uniform light output, attenuation length and are more prone to radiation damage. Use of pure meltstocks seems to improve the radiation hardness. It appears that the impurities have to be controlled at a level of ppb instead of ppm levels presently used. Clearly it is desirable to

	NaI	BGO	BaF_2	CsI	CeF_3	PbF_2
Density (g/cm^3)	3.67	7.1	4.89	4.51	6.16	7.77
Radiation Length (cm)	2.59	1.12	2.05	1.86	1.7	0.93
Molière Radius (cm)	4.4	2.7	4.3	3.8	2.6	1.8*
Photons/MeV (k)	40	8	10	18	4	C^v
% light in fast component	-	-	23	30	100	
Decay Const. Fast (ns)	-	-	0.6	10,36	5,30	C^v
Slow (ns)	230	300	620	1000	-	-
λ peak (nm) Fast	-	-	220	305	310,340	C^v
Slow	410	480	310	same	-	-
$\Delta L/\Delta T$ at 20°C (% / °C)	-	-1.55	**	-1.5	+0.08	
Radiation Damage♦ (kGy)	1	1	100	10	100	
Cost : SFr / ($R_M^2 \cdot X_0$)	120	60	120	50	-	10

C^v - Cerenkov radiator

* "apparent" Molière radius

** the slow component shows a variation of $\Delta L/\Delta T = -2.4$ % / °C.

♦ see discussion below

Table 2 : Properties of crystals.

identify and eliminate the impurities that lead to damage eg. Pb in BaF_2. Another possibility to improve the radiation hardness is to dope the crystals with elements that allow de-excitation of the trapping centres eg. Eu in BGO. Generally recovery takes place in most crystals with improvements seen over times ranging from hours to days. This may be undesirable as the calibration would then depend on the running conditions. More work on the radiation damage of full size crystals is clearly required.

For use at the LHC, in addition to other undesirable properties, NaI and BGO are sensitive to radiation damage at relatively low doses (~ 1000 Gy). Small samples of BaF_2 have been shown to be radiation resistant up to photon doses of 10^5 Gy. Recent measurements [42] on the radiation resistance of CeF_3 show a loss of only ~ 5 (33) % in transmission for doses of ~ 10^4 ($5\ 10^5$) Gy. Samples of a size of ~ 1 cm^2x 8 cm were used. Undoped CsI crystals of a diameter and length of 2.54 cm have recently been irradiated using γs from ^{60}Co [43]. The absorption coefficient increased by 0.05 / cm for a dose of $1.5.10^4$ Gy. The levels of radiation damage given here are those at the wavelength of emission of the fast component. It is believed that with further work the radiation resistance of most crystals can be improved. Both BaF_2 and CeF_3 appear to be able to operate at 10^4 Gy /year.

The slow component of BaF_2, accounting for ~80% of the total emission, has not only a decay constant of 600 ns but also a strong temperature dependence. Hence it has to be strongly suppressed. It can be filtered out by using a "solar blind" CsTe photocathode as the peak emission wavelengths of the fast and slow components are different. A fast / slow intensity ratio of ~ 1 can be achieved as can be seen from Table 3 [44]. These have been measured using 20 ns and 1 μs gates with the corrections applied for the additional slow component outside the 1 μs gate. The slow component can also be suppressed by doping BaF_2 with a small amount of

lanthanum (Table 3). Hamamatsu have recently developed a K-Cs-Te photocathode which has a sharper cutoff against the slow component [45]. The relative quantum efficiency curves of the two photcathodes as a function of wavelength indicate that a fast to slow ratio of 1: 0.1 can be achieved with K-Cs-Te. Doping may then become unnecessary. Most of the light in the fast component is sacrificed in the suppression of the slow component. A photoelectron yield from the fast component of ≥ 50 p.e./MeV is expected using the K-Cs-Te photocathode. Vacuum photodiodes with quartz windows are proposed for the readout though some gain may be necessary. Even further suppression of the slow component is required and is obtained by pulse shaping. The readout of BaF_2 with such a technique is non-trivial and will be expensive.

Photocathode Sample :	Bialkali		CsTe	
	Fast	Slow	Fast	Slow
BaF_2	1.00	6.20	0.54	0.68
BaF_2 : La (1%)	0.76	1.52	0.55	0.46
BaF_2 : La (20%)	0.48	0.48	0.24	0.16
BaF_2 : Tm (1%)	0.77	1.40	0.40	0.29

Table 3 : Slow component suppression in doped BaF_2

Recently a promising readout device for the scintillation light of BaF_2 has been developed. This is based on the parallel plate avalanche chamber , PPAC [46] , where a thin film of CsI is deposited, under vacuum, on a metal substrate (Fig. 26). The quantum efficiency can be increased, eg. from 20% to ~ 30% at 190 nm, by forming an adsorbed layer of TMAE. This also renders the photocathode less sensitive to contact with air. There is practically no sensitivity to the slow component of BaF_2 and hence drastic suppression of the slow component is not required. These chambers can be operated with or without gas gain. Without gain the yield of photo-electrons is small (~10000 p.e.'s /GeV) and the energy equivalent of the electronic noise could be large. Use of high gain leads to a reduced response with irradiation as the ion bombardment gradually destroys the photo-cathode. These aspects are currently being investigated.

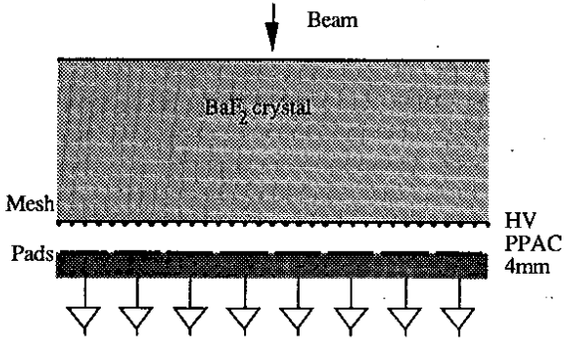

Figure 26 : Schematic of a parallel plate avalanche chamber used to read-out a preshower counter.

The emission wavelengths of the slow and the fast components in undoped CsI overlap significantly [43]. Hence the slow component cannot be reduced by filtering but short decay constants (2 and 20 ns) have recently been measured for light emission from CsI(Br) [47]. The sizeable temperature dependence of the light yield of CsI will require precise temperature monitoring. This is potentially a serious drawback in a large system.

CeF_3 , a newly found scintillator [48], has short radiation and Molière lengths, does not have a slow component and shows a very small temperature dependence of the light yield. The absence of the slow component may allow the use of Si photodiodes with the radiation damage of Si kept in mind. CeF_3 is not yet available in large enough quantities and more work, especially on the part of industry, is required before it can be considered for large scale calorimetry.

All the crystals mentioned so far are expensive and the demand for them is driven by HEP. Large volume production will require considerable initial investment. The necessary size of the inner radius may thus may not allow their use in a first generation LHC experiment.

Recently there has been renewed interest in Cerenkov radiators like PbF_2 [49] and KRS-6 [45]. Their very short radiation and Molière lengths coupled with low cost makes them attractive. Recent tests on the radiation damage of PbF_2 showed disappointing results but complete recovery from the effects of a dose of $4 .10^3$ Gy was observed after exposure to UV light for 10 minutes. However permanent damage was observed for a dose of 4.10^4 Gy. The light yield is usually low and photodevices with gain are necessary. Measurements in PbF_2 yield ~ 1300 photoelectrons / GeV leading to a resolution of ~ $3\%/\sqrt{E}$. Like CeF_3, PbF_2 is a material still under development by industry. Further investigation is clearly required.

From recent studies of scintillation properties and radiation damage mechanisms in several scintillators [45], it may be possible to "design" a scintillating glass, probably in the fluoride family, with the desirable properties of a short radiation length and a short decay constant but most significantly of all low cost. Tests on small samples of several heavy fluoride glasses have already started and preliminary radiation tests are encouraging. The R&D on these glasses should be vigorously pursued.

In summary, BaF_2 and CeF_3 appear to be able to meet the required performance. CeF_3 due to its shorter radiation and Molière lengths, absence of any slow component and better mechanical properties appears to be more promising but large scale production has still to be established. If a large volume is required then cost and availability may become the dominant selection criterion. New heavy scintillating or Cerenkov emitting glasses may resolve this but much more R&D work is required.

2.9 Noble Liquids

Recently the use of noble liquids like xenon (LXe) and krypton (LKr) has evoked a great deal of interest. The energy measurement can be carried out by collecting the ionisation

electrons and/or collecting the scintillation light. The best results for energy resolution with these liquids have been obtained with LKr [50] using charge read-out. An active volume given by a cylinder of diameter of 42 cm and a length of 76 cm led to an r.m.s. energy resolution of 1.7 % for positrons of an energy of 1.2 GeV.

The main advantages of this technique are :

- radiation hardness (probably limited by the hardness of the read-out elements),
- fast signals if scintillation light is used,
- ease of lateral and longitudinal segmentation,
- insensitivity to magnetic fields,
- modest purity is necessary if only the scintillation light is detected,
- yet to be demonstrated possibility of tuning e/π to 1 by exploiting the different decay constants for lightly and heavily ionizing particles.

The drawbacks are :

- cost and availability (for xenon),
- not much experience even at the level of a prototype of a size that can contain high energy electromagnetic showers,
- need for a cryostat leading to material in front of the calorimeter,
- for light readout the non-uniformity of light collection may lead to a sizeable constant term,
- difficulty in obtaining longitudinal segmentation and good two gamma separation if using the light readout only,
- complexity if a combined light and charge readout is used.

The relevant properties of the liquids are listed in Table 3.

	LAr	LKr	LXe
Density (g/cm^3)	1.39	2.45	3.06
Radiation Length (cm)	14.3	4.76	2.77
Molière Radius* (cm)	7.3	4.7	4.1
Photons/MeV (k)	40	40	40
% light in fast component	8	1	77
Decay Const. Fast (ns)	6.5	2	2
Slow (ns)	1100	85	30
λ_{peak} Fast (nm)	130	150	170
V_{drift} (10kV/cm) cm/μs	0.5	0.5	0.3
Temperature °K	94	124	160
Cost : SFr / ($R_M^2 \cdot X_0$)	-	55	150

* PDG definition

Table 3 : Properties of some noble liquids.

Of the noble liquids, LXe has the shortest radiation length, the shortest scintillation decay constant, the highest emission wavelength and the highest temperature. LXe is a scintillator

with a light output which is ~20 times larger than found in the fast component of BaF_2. Although the electron drift velocity in LXe saturates at a relatively low electric fields it is too small for use at the LHC. A factor ~ 6 increase in the drift velocity has been achieved by doping liquid Xe with a small quantity (7.10^{19} mols/cm^{-3}) of butane [51]. Small drift gaps and short bipolar shaping time may allow a reasonably fast response. The effect of radiation damage to the molecular solutes has still to be investigated.

The light collection method allows, in principle, a fast total energy measurement. The major difficulty here is the point to point uniformity of light collection. The individual calorimeter cells may have to be long, since the radiation length of LXe is fairly large, and narrow as fine granularity is important. Most of the light will thus have to suffer several reflections. Surfaces of high reflectivity to 170nm light are needed. Non-uniformity of light collection has to be minimized as it can lead to a sizeable constant term. Another problem may be the availability of LXe in a sufficiently large quantity. The lower cost and easier availability of LKr makes it an interesting candidate. It may be possible to add a small amount of LXe as a wavelength shifter to shift the light to a higher wavelength but more importantly to shorten the decay time constant. Though the Molière radius is not much larger than that for LXe, the radiation length is much larger thus aggravating the problem of the uniformity of light collection. A depth of ≥ 120 cm for an electromagnetic calorimeter at the LHC would probably only be acceptable for a dedicated experiment. An energy resolution of ~ $4\%/\sqrt{E}$ is attainable in a sampling mode if ≥ 50% of the shower energy can be deposited in LKr. Increasing this fraction would lead to even better energy resolution.

Two readout schemes are currently being pursued. The first one [52] uses self supporting trapezoidal cells with walls made out of thin (~ few hundreds of μm) UV reflecting Al foils (Fig. 27). The light readout elements are large area UV sensitive Si photodiodes immersed in the liquid. The results obtained so far come from tests using small volumes of LXe. These are :

- a quantum efficiency ~1 for light of a wavelength of 170 nm [53],
- development of fast amplifiers with a peaking time of 10 ns and a dynamic range of ~ 10^5 [52],
- an energy resolution below 1% for an energy deposit of ~2.65 GeV by 80 MeV/c ^{40}Ar ions [52],
- an attenuation length larger than 20cm [53].

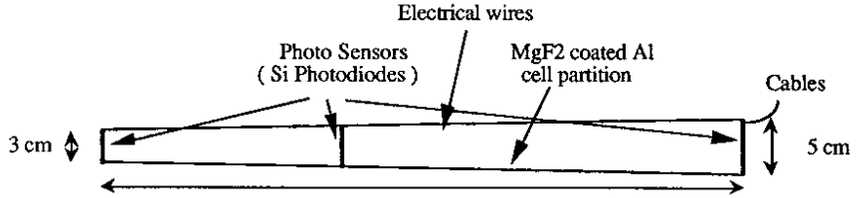

Figure 27 : A single cell of the scintillating liquid xenon detector, showing 3 photodiodes, UV reflector and cables.

The second scheme [53] combines light and charge read-out and should be able to achieve a better energy resolution and, perhaps more importantly, a smaller constant term as the two measurements are essentially independent. An illustration of a single cell is shown in Fig. 28. Deposited on the side walls is the (CsI+TMAE) photocathode described in the previous section. The photo-electrons, ejected by the scintillation light incident on these walls, are injected into the liquid. A fast signal is induced the moment the electrons leave the surface. The charge from the shower and the photocathode drifts across the gap and is digitized to determine the position of the shower in two dimensions. Excellent two gamma separation and determination of the direction ($\leq$ 1 mrad) is potentially possible. However the low drift velocity means that information from many events and crossings has to be unravelled. It is not yet clear whether such a scheme can work satisfactorily at high luminosities, even with a factor ~ 6 increase in drift velocity from doping. A full simulation has to be carried out. The main experimental results obtained [53] so far are :

- observation of the anti-correlation of light and charge signals previously seen by Doke et al. [54],
- measurement of the photon yield of $(30.9 \pm 3.0).10^3$ MeV^{-1},
- a free electron lifetime in excess of ~ 150 μs [55],
- an energy resolution using a charge readout of LAr of $\sigma \sim 1.2\%$ at 1 GeV.

Photo-electron injection into the liquid from a CsI+TMAE photocathode has still to be demonstrated.

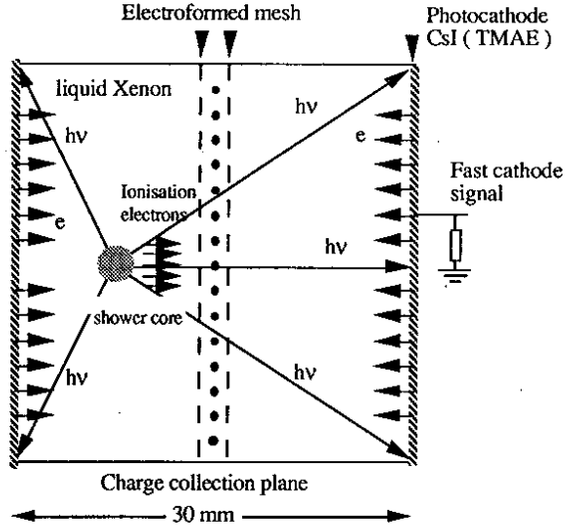

Figure 28 : Schematic of a cell for light and charge readout in liquid xenon [52].

In summary, an energy resolution of $\leq 1\% / \sqrt{E}$ appears to be possible but the smallness of the constant term, with implementation of directional and two shower separation capability, is

probably the real test for such techniques. Large prototypes of both schemes are planned and the results should be available within one to two years. A significant problem may be the availability of LXe in a sufficiently large quantity (LKr is a factor of ~ 10 more abundant). A quantity of 15 m^3 of LXe can be procured by 1999 at a price of 2.5 M\$/m^3 if a sufficient guarantee is given for the production to start in 1991 [52]. It is believed that a quantity of ~20-40 m^3 is required to have confidence of achieving the intended physics goals.

2.10 Front-end Electronics.

A fine granularity ($\approx$ .02 x .02) over a large geometric acceptance ($|\eta| < 3$) requires a large number of independent cells ($\approx 10^5$) and an even larger number of electronics channels if the calorimeter is subdivided in depth. The electronics must have a large bandwidth to cope with the 15 ns bunch crossing interval.

Each channel has to span a large dynamic range. The maximum is set by the possible observation of a new heavy vector boson decaying into an electron pair (1.7.1 above) Depending on the exact calorimeter granularity, the maximum energy in a cell will be ~1-2 TeV. The low end is determined by the muon peak ($\approx$ 300 MeV depending on the calorimeter longitudinal segmentation) and by the calorimeter noise ($\approx$ 30 MeV depending on the calorimeter technology). The consequent 16 bit dynamic range is large but the same precision is not needed over the whole range. It is sufficient to demand that the readout electronics not deteriorate the intrinsic calorimeter resolution and then a non-linear transfer function can be used [56]. Fig 29 shows, for two typical electromagnetic calorimeter resolutions, that an effective 10 bit dynamic range is adequate. In this example the electronics noise term was assumed to be a factor two lower than the intrinsic resolution term.

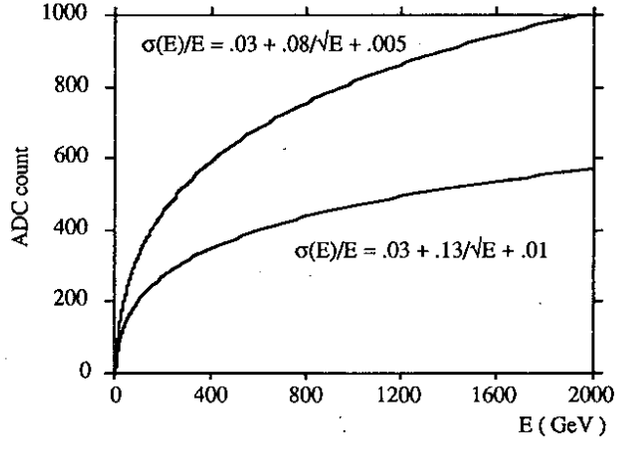

Figure 29 : Optimum transfer function for two typical electromagnetic calorimeter resolutions. An effective 10 bit dynamic covers the whole energy range In this example, the electronics noise is only half the calorimeter noise.

The temporal shape of the calorimeter pulses has already been discussed. Shaping will make the pulses from various calorimeters, using different techniques, similar and probably bipolar in shape (to minimize the base line shift) though the peaking times may vary from ≈ 10 to 50 ns. Some carry additional information eg. the pulse shape from the SPACAL fiber calorimeter allows discrimination of electrons from hadrons. A very fast sampling rate (≈ 7 ns) would be needed to exploit this characteristic [11].

The large amount of information from the calorimeter will have to be stored either in an analog [57] or a digital [56] form in a long (≈ 1 μs) pipe-line to wait for the trigger decision [12]. This pipeline device must have the same length for all detector components. It must run synchronously with the machine clock at the same or a multiple of the bunch crossing frequency. It may be worth noting that the experiments at HERA have already the problem of a trigger decision time greater than the bunch crossing time and all the information has to be stored in pipelines. Hence concepts working at 10MHz already exist.

Calorimeters will also have to provide data for the trigger. As the granularity required at the trigger level is much coarser, a summation over several calorimeter cells has to be carried out either in an analog or in a digital form. A fully digital architecture, consisting of non-linear transfer function at the digitization level, trigger summation and pipelining..., spurred stimulating discussions [56]. It was argued that most of the readout problems are similar to the ones that are being addressed by the high definition television industry [12].

To summarize, reading out such a large number of channels at high speed will be a formidable task. The practical consequences eg. the number of cables, power dissipation, electronics layout were not sufficiently studied at this workshop. A lot of the problems eg. length of pipelines, synchronisation etc. are probably common to all detectors and a close coordination will be required. The difficult problem of radiation hardness of the electronics is addressed by the Radiation Hardness Working Group.

3. CONCLUSIONS

The discussion in this paper has been guided by the physics potential of the LHC at luminosities in excess of 10^{34} cm^{-2} s^{-1}. This has resulted in very stringent requirements for the detection of electrons and photons in order to be able to detect the Standard Model Higgs particle if its mass lies in the range $80 \leq M_H \leq 1000$ GeV/c^2. In such a scenario the need for a very good hadronic energy resolution was less obvious and will in any case be compromised by pileup energy from minimum bias events. The calorimeter requirements at luminosities an order of magnitude lower than used above, eg. for higher cross-section precision experiments, will certainly lead to different conclusions. This should be studied. The effect of pileup has only been studied roughly. Triggers will select rare combinations of peculiar events and this effect should be studied further.

As far as the individual calorimeter techniques are concerned, none of them is presently at a point where one can state, with reasonable confidence, that it could work at the LHC at luminosities of 10^{34} cm^{-2}s^{-1} or more. Radiation damage of the calorimeter and its electronics must not be underestimated. The same is true for the implications of the large number of cells required, using electronics with a high bandwidth dissipating power ..etc. These practicalities have not been studied and may in the end decide the feasibility of a given calorimeter. Techniques suitable for forward calorimetry were not discussed at this workshop. Radiation hardness is the main criteria there. If it is confirmed that coarse calorimetry is good enough, a solution can probably be found.

Given the schedule for the construction of LHC, many participants felt that the time available is probably too short to develop completely new ideas for a first generation LHC detector. Major R&D effort on present, already proven, technologies by well organized and well supported groups is required. Such groups have been and are being formed and some of the questions that have been raised should have answers in the next two years.

Significant progress has been made since the ECFA Workshop at Barcelona last year. There is a much better understanding of the calorimeter performances required to answer the fundamental physics questions that can be tackled by the LHC. On the detector side, whereas at Barcelona many, frequently speculative ideas were presented, Aachen has seen positive results from new, medium to large scale, test experiments and, last but not least, the completion of the calorimeters for the HERA detectors.

A development which appears necessary is the availability of the proper computer aided engineering design tools which can predict, accurately and speedily, the performance change for a given design change. More effort in this direction is required in the near future so that the tools and trained experts are available in time for the optimization of LHC detectors. As subtstantial part of any LHC detector will probably be built by industry close collaboration is required both in the design and the construction phases.

Within the calorimeter working group, emphasis was put onto the detectors themselves, and very little on electronics, triggering and DAQ aspects. This has to change in the near future. These may be at least as difficult as the problems of the detector proper and may well in the end be the determining factors. How much of such an effort can be done generically and how much within a detector and even within a specific sub-detector has to be understood.

Given the short time available, the working group concentrated on the calorimeter techniques with little contact with other subgroups. It was frequently felt that it is not really possible to think of a calorimeter in the absence of the rest of the experiment. In order to progress further, it will soon be necessary to consider a complete detector in order to optimize the calorimeter performance.

Acknowledgements.

We would like to thank all the people, especially the sub-conveners, who contributed to the work of the Calorimetry Working Group.

References

[1] Proceedings of ECFA-CERN Workshop on the Large Hadron Collider in the LEP Tunnel, Lausanne and Geneva, March 1984, ECFA 84/85 and CERN 84-10 (1984).

Proceedings of the Workshop on Physics at Future Accelerators, La Thuile and Geneva, January 1987, CERN 87-07 (1987).

The Feasibility of Experiments at High Luminosity at the Large Hadron Collider, Ed. J.H. Mulvey, CERN 88-2 (1988).

Proc. DPF Summer Study on the Design and Utilization of the Superconducting Super Collider, Snowmass (Colorado) 1984 (AIP, NY, 1985).

Proc. 1986 DPF Summer Study on the Design and Utilization of the Superconducting Super Collider, Snowmass (Colorado) 1986 (Fermilab, Batavia, 1987).

Experiments, Detectors and Experimental Areas for the Supercollider, Ed. R. Donaldson, M.G.D. Gilchriese, Berkeley (1987).

Proceedings of the Workshop on Calorimetery for the Supercollider Ed. R. Donaldson, M.G.D. Gilchriese, University of Alabama, Tuscaloosa, Mar. 1989.

[2] ECFA Study Week on Instrumentation Technology for High Luminosity Hadron Colliders, September 1989, CERN 89-10, ECFA 89-124.

[3] Z. Kunzst and W. Stirling, Higgs Working Group, Vol 2, these proceedings.

[4] D. Froidevaux et al. Higgs Working Group, Vol 2, these proceedings.

[5] C. Seez et al., Higgs Working Group, Vol 2, these proceedings.

[6] F. Pauss, Beyond Standard Model Physics Working Group, Vol 1, these proceedings.

[7] M. Seymour, Higgs Working Group, Vol 2, these proceedings.

[8] L. Fayard, Top Working Group, Vol 2, these proceedings.

[9] P. Sphicas, SUSY Working Group, Vol 2, these proceedings.

[10] R. Barnett et al., LBL-27797 (1989)

[11] G. Goggi, Analysis of electron and pion pulses from the SPACAL calorimeter (Jul 1990)

[12] N. Ellis, L. Mapelli, S. Cittolin, Trigger and DAQ Working Group, Vol 1, these proceedings.

[13] J.P Repellin, Electron Identification Working Group, Vol 3, these proceedings.

[14] R. Apsimon et al., CERN PPE / 90-171 (1990).

[15] T. Akesson, Electron Identification Working Group, Vol 1, these proceedings.

[16] C. Wulz, Beyond Standard Model Physics Working Group, Vol 2, these proceedings.

[17] M. Della Negra et al., Higgs Working Group, Vol 2, these proceedings.

[18] L. Poggioli, Higgs Working Group, Vol 2, these proceedings.

[19] Radioactivation in LHC calorimeters, CERN/TIS-RP/90-18/CF G.R. Stevenson, Radiation Damage Working Group, Vol 3, these proceedings.

[20] T. Akesson et al., Nucl. Instr. and Meth. A241 (1985) 17.

[21] The ZEUS Detector, Status Report 1989, The ZEUS Calorimeter (Ed. E.Ros), Mar 1989 U.Behrens et al., Nucl. Instr. and Meth. A289 (1990) 115. A.Andresen et al., Nucl. Instr. and Meth. A290 (1990) 95.

[22] Influence of Instrumental effects on the performance of the ZEUS calorimeter, The ZEUS Calorimeter Group (presented by E.Ros), Proceedings of the Como Conference on Advanced Technology and Detectors (Como, Italy, 1990) (to be published in Nucl. Phys. A).

[23] A.Dwurazny et al., Nucl. Instr. and Meth. A277 (1989) 176.

[24] a) J. Fent et al., Nucl. Istr. and Meths. 225 (1984) 509.
b) M. Albrow et al., Nucl. Istr. and Meths. A256 (1987) 23.
c) B. Lohr et al., Nucl. Instr. and Meths., A254 (1987) 26.

[25] Kryshkin, Report to the Calorimetry Working Group, Aachen (1990). Kamyshkov, Report to the Calorimetry Working Group, Aachen (1990).

[26] U.Holm, Radiation Damage Working Group, Vol 3, these proceedings.

[27] A. Maio, Radiation Damage Working Group, these proceedings.

The Effects of Radiation Damage on a Scintillating Fiber Calorimeter, D. Acosta , LAA Preprint.

[28] F. Takasaki in Radiation Effects at the SSC, Ed. M. Gilchriese, SSC-SR-1035.

[29] L.Poggioli, Calorimetry Working Group, Vol 3, these proceedings.

Scintillating Fibre Calorimetry at the LHC. The SPACAL collaboration, CERN/DRDC/90-23

[30] G.Drews et al., Nucl. Instr. and Meth. A290(1990)335.

[31] P.Schacht, Results and Experience on LAr Calorimetry from H1, Contribution to the Working Group on Calorimetry at the 1990, ECFA-LHC Workshop, Aachen 1990.

[32] D. Fournier, Calorimetry Working Group, Vol 3, these proceedings.

Liquid Argon Calorimetry with LHC-Performance Specifications, B. Aubert et al., CERN/DRDC/90-32, Aug.90.

[33] J. Colas et al., The Electrostatic Transformer, Nucl. Instr. and Meth. A294(1990)583.

J. Colas et al., Analytical description of an EST, LAPP-EXP-90.07.
J. Colas, EST performances, Shower simulation, LAPP-EXP-90.08.

[34] V. Vuillemin, Calorimetry Working Group, Vol 3, these proceedings.

P.Cennini et al., Study of Liquid Argon Dopants for LHC Calorimetry, CERN/DRDC/90-35, Aug.90.

[35] E. Radermacher, Calorimetry Working Group, Vol 3, these proceedings.

[36] B.Mansoulie, Calorimetry Working Group, Vol 3, these proceedings.

[37] Shmakov, Calorimetry Working Group, Vol 3, these proceedings.

[38] J.P.Mendiburu, Calorimetry Working Group, Vol 3, these proceedings.

[39] E.Geulig et al., Warm Liquid Calorimetry for LHC, CERN/DRDC/90-50, Oct.90.

[40] G.Lindstroem, Calorimetry Working Group, Vol 3, these proceedings.

[41] G.Lindstroem, Radiation Damage of Silicon Detectors, Contribution to the Working Group on Calorimetry at the ECFA-LHC Workshop, Aachen 1990.

[42] D. Anderson, Private Communication.

[43] C. Woody et al., To be published in IEEE Trans. Nucl. Sci. NS-37 (1990).

[44] C. Woody et al. IEEE Trans. Nucl. Sci. NS-36 (1989) 536.

[45] P. Lecoq, Calorimetry Working Group, Vol 3, these proceedings.

[46] J. Seguinot et al., CERN EP/ 90-88.

[47] D. Renker, Talk on CsI given at ECFA Workshop, Aachen, 1990.

[48] D. F. Anderson, FNAL-Pub-89/169 (1989).

[49] D.F. Anderson et al. FNAL-Conf-90/46 (1990).

[50] V. M. Aulchenko et al., Novosibirsk Preprint 89-124 .

[51] K. F. Yoshino et al., Phys. Rev A14 (1976) 438.

[52] M. Chen et al., Calorimetry Working Group, Vol 3, these proceedings.

[53] T. Ypsilantis et al., Calorimetry Working Group, Vol 3, these proceedings.

[54] T. Doke, Experimental Techniques in High Energy Physics, Ed. T. Ferbel, Addison Wesley.

[55] D. Schinzel, Private Communication.
E. Aprile et al., Columbia Astrophysics Lab. No. 427 (1990).

[56] G. Goggi, B. Lofstedt, Trigger and DAQ Working Group, Vol 3, these proceedings.

[57] P.Jarron, ECFA-LHC Workshop, Aachen 1990.